Effect of temperature on the complexation of triscarbonatouranyl(VI) with calcium and magnesium in NaCl aqueous solution

Chengming Shang, Pascal E. Reiller

Effect of Temperature on the Complexation of Triscarbonatouranyl(VI) with Calcium and Magnesium in NaCl Aqueous Solution

*Chengming Shang and Pascal E. Reiller**

Université Paris-Saclay, CEA, Service d'Études Analytiques et de Réactivité des Surfaces (SEARS), F-91191 Gif-sur-Yvette CEDEX, France

Dalton Transactions **50**, 17165-17180

https://doi.org/10.1039/d1dt03204f

pascal.reiller@cea.fr

ABSTRACT

The complex formation of triscarbonatouranyl(VI) $UO_2(CO_3)_3^{4-}$ with alkaline earth metal ions Mg^{2+} and Ca^{2+} in 0.10 mol kg_w^{-1} NaCl were studied at variable temperatures: 5-30°C for Mg^{2+} and 10-50°C for Ca^{2+}. Under appropriate conditions, the ternary complexes ($M_nUO_2(CO_3)_3^{(4-2n)-}$ with n = 1 for Mg, n = {1;2} for Ca) were identified by time-resolved laser-induced luminescence spectrometry. Their pure spectral components at 50°C for $Ca_nUO_2(CO_3)_3^{(4-2n)-}$ and 30°C for $MgUO_2(CO_3)_3^{2-}$ were recovered by multivariate curve resolution alternating least squares analysis. Approximation models were tested to fit the experimental data — the equilibrium

constants of complexation measured at different temperatures — and deduce the thermodynamic functions, i.e., enthalpy, entropy, and heat capacity. The weak influence of temperature on complexation constants induces large uncertainties on thermodynamic functions. Assuming the enthalpy is constant with temperature using the Van't Hoff equation, the first stepwise complexation of $UO_2(CO_3)_3^{4-}$ by Ca^{2+} is estimated to be slightly endothermic with $\Delta_r^{VH}H°_m$ = (4.9 ± 5.9) kJ mol^{-1}, while the second stepwise complexation of $CaUO_2(CO_3)_3^{2-}$ by Ca^{2+} with is slightly exothermic $\Delta_r^{VH}H°_m$ = -(6.2 ± 13.3) kJ mol^{-1}. In contrary to Ca^{2+}, the complexation of $UO_2(CO_3)_3^{4-}$ by Mg^{2+} is slightly exothermic with $\Delta_r^{VH}H°_m$ = -(11.7 ± 10.3) kJ mol^{-1}. These values are not significantly different from zero inasmuch as the uncertainties are important due to a weak dependence of $\log_{10}K°$ values. The entropic character of the complexation is verified as $T\Delta_rS°_m$ = (36.5 ± 6.0) kJ mol^{-1} for the first stepwise complexation of $UO_2(CO_3)_3^{4-}$ by Ca^{2+}, $T\Delta_rS°_m$ = (13.8 ± 13.3) kJ mol^{-1} for the second stepwise complexation of $CaUO_2(CO_3)_3^{2-}$ by Ca^{2+}, and $T\Delta_rS°_m$ = (14.2 ± 10.3) kJ mol^{-1} for the complexation of $UO_2(CO_3)_3^{4-}$ by Mg^{2+}. The energetics of complexation and sensitivity analysis of model estimates with temperature are discussed. The uranium speciation in the case of the safety of nuclear waste management, using the present thermodynamic functions, provides support to the assessment of underground nuclear waste repositories.

Introduction

The migration of actinides in natural environments, especially uranium, is of great importance in the long-term performance assessment of nuclear waste processing and disposal [1]. It is thus necessary to acquire the environmental information of the geological repository — temperature, pH value, nature of solid phases, types of existing inorganic and organic complexing agents, *etc.* —, which influences the mobility of radionuclides. With this aim in mind, the thermodynamic constants — formation constant $\log_{10}K°$—, and functions — Gibbs energy

$\Delta_r G°_m$, enthalpy $\Delta_r H°_m$, entropy $\Delta_r S°_m$, heat capacity $\Delta_r C_p°_m$, *etc*. — for involved reactions are mandatory for the predictive calculations. The complexation of actinides by major inorganic materials in underground waters at other temperatures than standard raises critical scientific interest, because the temperature in the nuclear waste storage casks could be up to 90°C because of radioactive decay [2-3]. However, a certain lack of knowledge on thermodynamic parameters of actinide complexation with temperature renders it difficult to predict chemical behaviour of actinides in the near-field of radioactive waste repositories, where a significant temperature gradient is estimated in timescale evolution [4]. The variation of water properties with temperature, *e.g.*, ion product and dielectric constants, can result in significant rearrangement of the solvation sphere of complexing ions, affecting the energetics of uranium complexation reactions [5-6]. Therefore, full thermodynamic data of uranium reactions with various common ligands like carbonate are of interest to accurately simulate the uranium transport in the near-field, as well as in the far field, of a repository [7].

The nuclear waste repository isolation system consists typically of a natural barrier, mainly in clay or granite, depending on the country-specific rock formation, and an engineered barrier including in general waste canister, bentonite backfill, and concrete liner [8]. This multi-barrier system is extremely important in preventing the migration of actinides into the biosphere by means of pore-waters, which are similar in compositions with Cl^-, SO_4^{2-}, HCO_3^-, Ca^{2+}, Mg^{2+}, and Na^+ as the main ions at pH value *ca.* 8 in several envisaged geological formations [9-14].

The triscarbonatouranyl(VI) complexes with alkaline earth metals (Mg^{2+}, Ca^{2+}) have been reported, or calculated, in the literature as one of the predominant U(VI) species under a variety of conditions at near-standard temperatures [15-20], even if U(IV) phases are controlling the solubility [20]. The formation constants of these complexes have been determined around standard temperature using different techniques, *e.g.*, time-resolved laser-induced luminescence spectrometry (TRLFS) [21-25], Ca^{2+} selective electrodes [18], anion exchange

[26-27], and ultraviolet-visible (UV/Vis) absorption spectroscopy [28-29]. Their molecular structures have also been well defined by EXAFS [19,21-22,30-31] and molecular simulations [32-33]. In recent works [34-36], we have reported the determinations of the stepwise thermodynamic constants $\log_{10}K°_{n}$ for the equilibria,

$$M^{2+} + UO_2(CO_3)_3^{4-} \rightleftarrows MUO_2(CO_3)_3^{2-}$$

$$M^{2+} + CaUO_2(CO_3)_3^{2-} \rightleftarrows M_2UO_2(CO_3)_2(aq)$$

where M^{2+} represents the divalent alkaline earth free ion Mg^{2+} and Ca^{2+}, and the cumulative thermodynamic constants $\log_{10}\beta°_{n.1.3}$ for the equilibria,

$$nM^{2+} + UO_2^{2+} + 3CO_3^{2-} \rightleftarrows M_nUO_2(CO_3)_3^{(4-2n)-}$$

(n = 1 for Mg, and n = {1;2} for Ca)

in NaCl and $NaClO_4$ electrolytes using TRLFS. We also obtained their specific interaction coefficients $\varepsilon(M_nUO_2(CO_3)_3^{(4-2n)-},Na^+X^-)$ (X^- being Cl^- and ClO_4^-) using the specific ion interaction theory (SIT) that were absent from compilation of data [37-39] — see our previous works [34-36] and references therein. Using these data, the thermodynamic functions of the ternary complexes under standard conditions are more complete and the speciation modelling should be more reliable.

However, very scarce data at varying temperature are available for $M_nUO_2(CO_3)_3^{(4-2n)-}$ complexes. Endrizzi & Rao [18] measured the complexation of $Ca_nUO_2(CO_3)_3^{(4-2n)-}$ complexes at 25°C using calorimetric titration. They concluded that the successive formations are entropy driven, and the contribution from enthalpy is rather small with $\Delta_r H°$ = -(7.6 ± 5.8) and (0 ± 7) kJ mol^{-1} for $CaUO_2(CO_3)_3^{2-}$ and $Ca_2UO_2(CO_3)_3(aq)$, respectively, and statistically no different from zero. Similar conclusions were reported using calorimetry by Jo *et al.* [28] with $\Delta_r H°_m$ = -(1.2 ± 0.3) and -(3.1 ± 3.0) kJ mol^{-1} for $CaUO_2(CO_3)_3^{2-}$ for $Ca_2UO_2(CO_3)_3(aq)$, respectively. The latter authors reported the equilibrium constants at variable temperatures (10-70 °C) using

TRLFS, Ca^{2+} selective electrode, UV/Vis absorption spectroscopy, and calorimetry. However, the experimental performance of the used techniques was limited to 70°C. For this reason, the experimental results measured in the temperature range of 10-50°C, though incomplete, were applied to the modified isoelectric reactions, as defined in Eq. 15 and Eq. 16, in order to extrapolate the $\log_{10}K°_{n.1.3}$ to 70°C and derive the enthalpies using the Van't Hoff equation. The enthalpies of reaction were determined to be $\Delta_r H°_m$ = -1.2 kJ mol^{-1} and -1.7 kJ mol^{-1} for $CaUO_2(CO_3)_3^{2-}$ and $Ca_2UO_2(CO_3)_3$(aq), respectively, in satisfactory agreement with the results directly measured at 25°C by calorimetry. The application of isoelectric reaction to enlarge the validity of the Van't Hoff equation is particularly useful to predict the stability constants at non-standard temperature. The authors later applied the same analysis method to Mg-UO_2-CO_3 system and obtained $\Delta_r H°_m$ = (4.3 ± 1.5) kJ mol^{-1} for $MgUO_2(CO_3)_3^{2-}$ [29].

Recently, Maia*, et al.* [40], also using the Van't Hoff equation and a Schubert type method applied to an ion-exchange resin, reported $\Delta_r H°_m$ = (14.9 ± 5.1) kJ mol^{-1} and (36.5 ± 10.0) kJ mol^{-1} for $CaUO_2(CO_3)_3^{2-}$ for $Ca_2UO_2(CO_3)_3$(aq), respectively, slightly more important than the previous results [18,28]. One should question before any modelling the fulfilment of an important criterion of the Van't Hoff equation, the constant molar enthalpy in the investigated temperature range, as the derived parameters are very sensitive to the fitting values. Maia *et al.* [40] also reviewed the data of Jo *et al.* [28] by directly fitting the experimental values measured at 10-70°C to the Van't Hoff equation — not adopted in the original paper. Similar thermodynamic trends were obtained with the data of Jo *et al.* [28] — $\Delta_r H°_m$ = (10.9 ± 9.5) kJ mol^{-1} and (23.5 ± 7.0) kJ mol^{-1} for $CaUO_2(CO_3)_3^{2-}$ and $Ca_2UO_2(CO_3)_3$(aq), respectively — that could be attributed to the constant enthalpy assumption in absence of modification to isoelectric reactions.

In the present work, we will focus on the complexation of triscarbonatouranyl(VI) with Ca^{2+} and Mg^{2+} by TRLFS in the temperature range 10-50°C and 5-30°C, respectively. Stability constants of $M_nUO_2(CO_3)_3^{(4-2n)-}$ will be determined at I_m = 0.1 mol kg_w^{-1} NaCl, with

spectroluminescent titration by Ca^{2+} or Mg^{2+} at variable pH values, which has been successfully applied to determine formation constants and interaction coefficients in our previous studies [34-36]. The luminescence emission intensity and decay-times with increasing temperatures will also be studied. Different approximation models — the Van't Hoff equation, the constant heat capacity model, the DQUANT equation, and the isoelectric modification — will be adjusted to our experimental values. The molar enthalpy values obtained in different approaches will be compared with previously published values [18,28-29,40]. The implications in complexation mechanisms will be further discussed, in combination with our previous observations in concentrated electrolytes. These data can serve as parameters in the prediction of uranium migration in deep underground geological nuclear waste management context. Coupled influence of temperature and ionic strength on $M_nUO_2(CO_3)_3^{(4-2n)-}$ complexation will be analysed for particular scenarios in combination with our previous data [34-36].

Materials and Methods

Sample preparation

The stock solution of U(VI) was prepared by dissolving high purity U_3O_8 in 37% hydrochloric acid (Sigma-Aldrich, ACS reagent). Inductively coupled plasma mass spectroscopy (ICP-MS) was used to measure the stock concentration of U(VI). The concentration of U(VI) in all studied solutions was fixed at 50 μmol kg_w^{-1}. The ionic strength was maintained at 0.1 mol kg_w^{-1} with anhydrous NaCl (Sigma-Aldrich, ACS reagent, ≥ 99%) and Millipore deionized water (Alpha-Q, 18.2 MΩ cm). The addition of freshly prepared $NaHCO_3$ (Analytical Grade, Fisher) solution was previously calculated considering the equilibrium between the atmospheric CO_2 and the aqueous pH value at 25°C. Calcium chloride ($CaCl_2$, Sigma-Aldrich, ACS reagent, ≥ 99%) and magnesium chloride ($MgCl_2$, Sigma-Aldrich, ACS reagent, ≥ 99%) were used to control the concentrations of alkaline earth metal ions. Freshly prepared NaOH (Analytical Grade, Fisher) and diluted HCl solutions were used for the pH adjustments. The samples were undersaturated

with respect to uranium (UO_3:$2H_2O$ or β-$UO_2(OH)_2$) [39], and calcite [41] (for Ca-series) or magnesite [42] (for Mg-series). No obvious precipitation was observed throughout the experiments. The preparation of all samples was carried out by weighing under aerobic conditions.

The pH measurements were done using a combined hydrogen ion-sensitive glass electrode (Mettler Toledo, USA), filled with saturated potassium chloride (Radiometer Analytical, HACH). The recommended pH buffer solutions by National Institute of Standards and Technology (NIST) (pH 1.68, 4.01, 6.87, and 9.18 at 25°C, SI Analytics, Mainz, Germany) were used throughout the experiments. The detailed information of the commercial buffer solutions can be found in the literature [43] — see Table S1 of the Supplementary Information (ESI) —, and the corresponding pH values at other temperatures are in Table S2 of the ESI. The pH buffers and the sample solutions were maintained in a water bath (Lauda Ecoline E100, Germany) operating at the desired temperature. The default temperature on the pH meter (Mettler Toledo, USA) was manually reset before performing the calibration at other temperatures. Four-point calibrations based on the linear relationship between the pH values of buffer solutions and the potential read on the pH-meter were achieved in 5-50°C temperature range (see Figure S1 of the ESI). The sample bottle was placed in a beaker containing the water at the desired temperature in order to maintain the solution temperature during pH measurements. The pH values were regularly adjusted if there were any modifications prior to the luminescent spectrum acquisition. The pH measurements were performed in triplicate for each sample.

Time-resolved laser-induced luminescence spectroscopy

The time-resolved luminescence apparatus has been already described [34-36,44]. The sample solution was added in a fluorescence quartz cuvette with a sealable cap (QS 117F, Suprasil, Hellma Analytics) leaving a minimum headspace to limit evaporation and CO_2 degassing. Before spectrum acquisition, the cuvette was placed in the thermostated sample

holder during at least 20 min. The temperature was maintained at a constant value by circulating water through the thermostat (Peter Huber Kältemaschinenbau AG, Germany). The sample cuvette was thermally equilibrated with the circulating water throughout the measurements for minimizing the temperature fluctuation on uranyl fluorescence. The laser excitation source in this study is a frequency-tripled Nd:YAG laser at 355 nm (Surelite, Continuum, USA) providing a 5 ns pulse at 10 Hz of about 170 mJ as energy. An optical parametric oscillator system (Horizon, Continuum, USA) was used to tune the excitation wavelength at λ_{exc} = 450 nm. The fluorescence beam energy — average of 100 laser shots — was read on a Joule-meter RJP-734 (Laser Probe, Inc.). The 300 lines per mm grating was selected in monochromator spectrometer (Acton). The resulting measured fluorescence signal, recorded at a delay time D = 25 ns with the gate width W = 1 µs, was detected by an intensified CCD camera (Andor, UK) maintained at -10°C by Peltier effect.

The recorded spectra were integrated over the emission wavelength range at varying D values, with the trapezoidal method implemented in Origin 9.0 software (OriginLab Corporation, USA), to evaluate the fluorescence intensity at various delay times. The least-square fitting process (Levenberg-Marquardt algorithm) was used to calculate the luminescence intensity at $D = 0$ and decay-time τ by fitting the intensity results to the exponential fluorescence decay function, expressed as already discussed [34-36],

$$FI = \sum_i FI_0 \, \tau_i \exp\left(-\frac{D}{\tau_i}\right)\left(1 - \exp\left(-\frac{W}{\tau_i}\right)\right) \quad (1)$$

where FI and FI_0 are respectively the fluorescence intensity at a specific delay time and at D = 0. The gate width W = 1 µs and τ_i represents the decay-time of species i.

Equilibrium constants and ionic medium corrections

The stoichiometry of $M_nUO_2(CO_3)_3^{(4-2n)-}$ complexes is identified by the so-called slope analysis, which has been successfully applied in our previous studies [34-36], to calculate the formation

constants in NaCl and $NaClO_4$ electrolytes of different ionic strengths. The pH values and Mg^{2+}/Ca^{2+} concentrations are changed simultaneously in spectroluminescent titration i) to avoid the occurrence of $UO_3{:}2H_2O$(cr) [38-39] and calcite ($CaCO_3$) [41] or magnesite ($MgCO_3$) [42] compared to the typical pH-fixed experimental methodology, and ii) to allow the formation of ternary species to a great magnitude in solution.

Successive formations of $M_nUO_2(CO_3)_3^{(4-2n)-}$ are described with the conditional equilibrium constants $K_{n.1.3}$ expressed as follows,

$$nM^{2+} + UO_2(CO_3)_3^{4-} \rightleftarrows M_nUO_2(CO_3)_3^{(4-2n)-}$$

$$K_{n.1.3} = \frac{\left[M_nUO_2(CO_3)_3^{(4-2n)-}\right]}{[M^{2+}]^n[UO_2(CO_3)_3^{4-}]} \qquad n = 1, 2 \tag{2}$$

where squared brackets indicate concentration in molality (mol kg_w^{-1}).

The logarithmic transformation of Eq. 2 in Eq. 3 allows calculating the $\log_{10}K_{n.1.3}$ value. The slope *n* in Eq. 3 stands for the stoichiometry of Mg^{2+}/Ca^{2+}, R_f is the concentration ratio between complexed and non-complexed $UO_2(CO_3)_3^{4-}$ by Mg^{2+}/Ca^{2+}. The intercept $\log_{10}K_{n.1.3}$ refers to the conditional stepwise formation constants of $M_nUO_2(CO_3)_3^{(4-2n)-}$ at a given ionic strength,

$$\log_{10} R_f = \log_{10} \frac{\left[M_nUO_2(CO_3)_3^{(4-2n)-}\right]}{[UO_2(CO_3)_3^{4-}]/_\alpha} \tag{3}$$

which can be converted to luminescence intensity supposing it is proportional to the U(VI) concentrations.

$$\log_{10} R_f = \log_{10} \frac{FI_0\left(M_nUO_2(CO_3)_3^{(4-2n)-}\right)}{FI_0(UO_2(CO_3)_3^{4-})/_\alpha} \tag{4}$$

Here $FI_0(M_nUO_2(CO_3)_3^{(4-2n)-})$ is the fluorescence intensity extrapolated at $D = 0$. $FI_0(UO_2(CO_3)_3^{4-})$ is the one of the non-complexed $UO_2(CO_3)_3^{4-}$ at pH 9, and α represents the Ringböm coefficient [45] of $UO_2(CO_3)_3^{4-}$. The variation of $UO_2(CO_3)_3^{4-}$ with pH at $[M^{2+}] = 0$ conditions was calculated to assess the value of α — the reader is referred to previous papers

for detailed explanation and specific calculation [34-36]. The α values were calculated using the thermodynamic data ($\log_{10}K°$ and $\Delta_r H°_m$) from Table S3 of the ESI [38], and specific ion interaction coefficients from Table S4 of the ESI [34,36,38]. As the H^+ activity was determined from the acidity measurement of the solutions, the dissociation constants of water pK_w, were used to evaluate the H^+ concentration at various temperatures [5]. The corresponding α values at each specified aqueous condition was listed in Table S5 of the ESI.

The specific ion interaction theory (SIT) was used to correct the ionic strength effect in solution, as recommended in widely accepted Nuclear Energy Agency-Thermochemical Data Base (NEA-TDB) reviews [37-39]. The activity coefficient γ_i of an aqueous species i in the SIT approach is given by

$$\log_{10} \gamma_i = -z_j^2 D_H + \varepsilon(j, k, I_m)\, m_k \quad (5)$$

with $D_H(T)$ the temperature-dependent Debye-Hückel term expressed as,

$$D_H(T) = \frac{A(T)\sqrt{I_m}}{1+1.5\sqrt{I_m}} \quad (6)$$

where z_i is the charge of ion i, $\varepsilon(j,k,I_m)$ ($kg_w\ mol^{-1}$) is the ion interaction coefficient between the aqueous ion j and ion k of background electrolyte of concentration I_m at a given temperature — in this study no variation of ε with I_m was postulated and is thus considered $\varepsilon(j,k)$ in the following. The temperature influence on $\varepsilon(j,k)$ ($kg_w\ mol^{-1}$) is usually not available for the involved ions. However theoretically, $\varepsilon(j,k)(T) = \varepsilon(j,k)(T°)T°/T$ because $\varepsilon(j,k)m_k$ is a second virial expansion term [46-47]. In the experimental temperature range, the correction of $\varepsilon(j,k)m_k$ to temperature is not necessary as the correction should be too small to be considered. Values of the Debye-Hückel parameters A(T) at different temperatures are shown in Table S6 of the ESI. The relationship between conditional formation constants and ionic strength is expressed by

$$\log_{10} K_{n.1.3} = \log_{10} K^{\circ}_{n.1.3} + \Delta z^2 D_H - \Delta\varepsilon I_m \quad (7)$$

where

$$\Delta z^2 = z\left(M_nUO_2(CO_3)_3^{(4-2n)-}\right)^2 - n\,z\left(M^{2+}\right)^2 - z\left(UO_2(CO_3)_3^{4-}\right)^2 \quad (8)$$

(Δz^2 = -16 for n = 1 and Δz^2 = -24 for n = 2) and

$$\Delta\varepsilon = \varepsilon\left(M_nUO_2(CO_3)_3^{(4-2n)-}, Na^+\right) - n\varepsilon\left(M^{2+}, Cl^-\right) - \varepsilon\left(UO_2(CO_3)_3^{4-}, Na^+\right) \quad (9)$$

with the used values of ε(j,k) listed in Table S4 of the ESI.

Temperature dependence modelling

The formation constants for many chemical species are tightly related to temperature. However, thorough understanding of the temperature-dependent chemical behaviour of $M_nUO_2(CO_3)_3^{(4-2n)-}$ complexes has not yet been developed because of the scarcity of experimental results at higher than standard temperatures [39]. Nonetheless, computational methods such as the constant enthalpy equation, the constant heat capacity equation, the DQUANT model and the modification to isoelectric reactions have been proven adequate in a certain temperature range for evaluating temperature-dependent complexation constants. These four models were employed to describe the temperature-dependent $\log_{10}K°_{n.1.3}$ measured in the temperature range 10-50°C for $Ca_nUO_2(CO_3)_3^{(4-2n)-}$ and 5-30°C $MgUO_2(CO_3)_3^{2-}$ and used to cautiously extend their formation constants at higher temperatures. The simplified Van't Hoff equation, assuming constant $\Delta_rH°_m$ with temperature and zero heat capacity, is shown in Eq. 10.

$$\log_{10} K°(T) = \log_{10} K°(T_0) - \frac{\Delta_r H°_m(T_0)}{R\ln(10)}\left(\frac{1}{T} - \frac{1}{T_0}\right) \quad (10)$$

with $K°$ the formation constant under standard conditions (infinite dilution), R the gas constant (8.31451 J K^{-1} mol^{-1}), T the absolute temperature in Kelvin, and $\Delta_rH°_m(T_0)$ the molar reaction enthalpy at standard temperature T_0. It should be noted that the validity of temperature range $(T-T_0) \leq 10$ K is quite narrow in this equation [48]. Extrapolation over a

temperature range larger than 10 K will undoubtedly introduce greater uncertainties in the resulted $\log_{10}K°(T)$.

The constant non-nil heat capacity equation slightly extends the validity of temperature range to 20 K (Eq. 11) [48]. The assumption of constant heat capacity is useful to calculate the equilibrium constant in the range 273-473 K. In some cases, the heat capacity term can be neglected if the entropy and the heat capacity are comparable in magnitude as the term of $\Delta_r C°_{p,m}[\Delta T - T\ln(T/T_0)]$ is less important than $\Delta_r S°_m \Delta T$.

$$\log_{10} K°(T) = \log_{10} K°(T_0) - \frac{\Delta_r H°_m(T_0)}{R\ln(10)}\left(\frac{1}{T}-\frac{1}{T_0}\right) + \frac{\Delta_r C°_{p,m}}{R\ln(10)}\left[\left(\frac{T_0}{T}-1\right)+\ln\left(\frac{T}{T_0}\right)\right] \quad (11)$$

Helgeson [49] reported the enthalpy- and entropy-based DQUANT model, as shown in Eq. 12.

$$\log_{10} K°(T) = \frac{\Delta_r S°_m}{RT\ln(10)}\left\{T_0 - \frac{\theta}{\omega}\left[1-\exp(\exp(b+aT) - C + \frac{T-T_0}{\theta})\right]\right\} - \frac{\Delta_r H°_m(T_0)}{RT\ln(10)} \quad (12)$$

where $\Delta_r H°_m$ represents the molal reaction enthalpy, $\Delta_r S°_m$ denotes the molal reaction entropy, a = 0.01875 K^{-1}, b = 12.741, c = exp (b + aT_0), θ =219 K and ω = (1 + acθ). The uncertainties of the formation constants determined for various chemical reactions using the DQUANT equation show less than 1-9% error in 0-200°C temperature range [48].

Isoelectric reactions are defined for the chemical reactions of the following form: the sum of positive charges among the reactants equals the total amount of positive charges among the products, and the same for the negative charges among reactants and products. The modifications of $M_nUO_2(CO_3)_3^{(4-2n)-}$ complexation to isoelectric reactions requires the additional equations Eq. 13 131313and Eq. 14 to balance out the charges in Eq. 2:

$$CO_2(aq) + H_2O \rightleftarrows CO_3^{2-} + 2H^+ \quad (13)$$

$UO_2^{2+} + 3CO_3^{2-} \rightleftarrows UO_2(CO_3)_3^{4-}$	(14)

The isoelectric forms of $M_nUO_2(CO_3)_3^{(4-2n)-}$ complexation are expressed as follows.

$$M^{2+} + UO_2^{2+} + 2CO_2(aq) + CO_3^{2-} + 2H_2O \rightleftarrows MUO_2(CO_3)_3^{2-} + 4H^+ \quad (15)$$

$$2M^{2+} + UO_2^{2+} + 3CO_2(aq) + 3H_2O \rightleftarrows M_2UO_2(CO_3)_3(aq) + 6H^+ \quad (16)$$

These kinds of reactions can cancel out the electrostatic contributions to the temperature dependence of enthalpy. The formation constants of the additional reactions Eq. 13 and Eq. 14 have been calculated for the temperature range of 5-90°C using the existing general formula [50-52], as listed in Table S3 of the ESI. The enthalpies for the isoelectric reactions Eq. 15 and Eq. 16 were calculated by the Van't Hoff equation with the assumption of constant enthalpy and zero heat capacity. In this study, the formation constants $\log_{10}K°_{n.1.3}(T)$ of $M_nUO_2(CO_3)_3^{(4-2n)-}$ were finally determined by subtracting the $\log_{10}K°(T)$ of Eq. 13 and Eq. 14 from the global equilibrium constants $\log_{10}\beta°_{n.1.3}(T)$ for the isoelectric reactions Eq. 15 and Eq. 16, estimated by the Van't Hoff equation at each temperature, as listed in Table S7 of the ESI. The values of $\log_{10}K°_{n.1.3}(T)$ ascertained by different computational approximations were compared considering the individual uncertainties involved in each model.

Results and Discussion

Luminescent emission spectra analysis

Fig. 1 and 2 illustrate the evolutions of luminescent emission spectra of $M_nUO_2(CO_3)_3^{(4-2n)-}$ complexes. The formation constants for $CaUO_2(CO_3)_3^{2-}$ were measured in temperature range of 10-50°C, while those for $MgUO_2(CO_3)_3^{2-}$ were achieved in a relatively narrower temperature range (5-30°C), because of a pronounced decrease in the luminescence emission intensity, and a strong deformation of characteristic spectra at T > 30°C that caused difficulties in interpreting the luminescence evolution.

At a specified temperature, the spectra showed an increase in the emission intensity with increasing alkaline earth metal concentrations, which indicates the successive complexation of Mg^{2+}/Ca^{2+} to $UO_2(CO_3)_3^{4-}$. As temperature increases, the global amplitude of intensity suffered a pronounced decrease. As shown in Fig. 3, the solution of fixed $[Ca^{2+}]$ = 6.13 10^{-4} mol kg_w^{-1}

displays an obvious decrease in intensity when the temperature increases from 40 to 50°C. Apparently, the increase in temperature leads to slight shifts of the spectra to longer wavelengths also broader characteristic bands. It is reasonable to deduce that the band shifts and broadening can become more significant even contributing to the deformation of spectra at higher temperatures outside the experimental range. One can observe that in the temperature range of 10-35°C, the samples exhibited well-defined characteristic spectra in the course of Ca-UO_2-CO_3 complexation, while outside this range, the spectra showed irregular evolution at the beginning of the complexation, *i.e.*, 40, 45, and 50°C.

In addition, the luminescence decay-times for the Mg and Ca species were evaluated at the investigated temperatures by averaging the measured decay-times of correspondent sample solutions that give the slope of 1 or 2 in the slope analysis. The values are listed in Table S8 of the ESI. For all three complexes $Mg/Ca_nUO_2(CO_3)_3^{(4-2n)-}$, remarkable decrease in their decay-times was observed with increasing temperature, representing the quenching behaviour. From 10 to 50°C, the difference in luminescence decay-times for $CaUO_2(CO_3)_3^{2-}$ and $Ca_2UO_2(CO_3)_3(aq)$ became smaller at higher temperatures, which verifies the occurrence of dynamic quenching effects. Furthermore, it was assessed that the Mg complex showed a fast decay-time compared to the Ca complexes at the same temperatures in 0.1 mol kg_w^{-1} NaCl, *e.g.*, $\tau(MgUO_2(CO_3)_3^{2-})$ = (25.80 ± 0.85) ns, $\tau(CaUO_2(CO_3)_3^{2-})$ = (48.52 ± 2.84) ns, $\tau(Ca_2UO_2(CO_3)_3(aq))$ = (64.13 ± 1.89) ns at 10°C — see Table S8 of the ESI for the values at 15°C and 22°C. This observation corroborates our previous results at 0.1 mol kg_w^{-1} $NaClO_4$ [35]. In terms of the complexes temporal properties, our experiences suggested that the luminescent capacity for the Ca(II)-bound U(VI) species are stronger than the Mg(II)-bound U(VI) species, which can be partially attributed to their structural differences at the molecular scale, such as the distance of the localization of Mg^{2+} and Ca^{2+} near $UO_2(CO_3)_3^{4-}$ group.

Specifically, we compared the area-normalized emission spectra of triscarbonatouranyl from 5 to 50°C in the absence of Mg^{2+}/Ca^{2+} in Fig. 4. The concentration of U(VI) varied from 50 to 250 µmol kg_w^{-1} in order to increase the luminescence at the highest temperatures. Indeed, the emission spectra contain features originating from vibronic transitions from the lowest excited state to the ground state manifold, 11→00 of the hot band and 10→0ν (ν = 0, 1, 2, 3) of other peaks [53]. With the increase in temperature, the less-defined bands of $UO_2(CO_3)_3^{4-}$ were continuously red-shifted.

Numerous reasons have been put forward in the application of laser techniques. The red-shifted and broadened with lower intensity emission spectra of $UO_2(CO_3)_3^{4-}$ may give impression that the non-radiative decay becomes more important at higher temperature, which lowers the quantum yield (Q). It is also possible that the rates of some reactions, *e.g.*, the formation of an internal charge-transfer (ICT) state, which hinders the radiative decay [54], may vary with temperature and contribute to the luminescent changes. Further research is needed to probe the luminescent properties of triscarbonatouranyl(VI) with temperature.

The evolution of spectral band positions with increasing [Ca^{2+}] allows sorting out individual spectra of involved species, notably at higher temperatures, *i.e.*, 40, 45, and 50°C, where the band shifts were obvious. The data analysis method employed in the present study is the combination of Singular Value Decomposition (SVD) [55], used to assess the number of distinguishable components, and multivariate curve resolution alternating least squares (MCR-ALS) [56-58] used to recover the spectra. The analysed global data matrix at a specified temperature is composed of 1024 rows and *n* columns, with 1024 corresponding to the number of pixels of the CCD camera (416.46-633.81 nm wavelength range), and *n* corresponding to the sample number in each series. The calculations have been carried out with codes developed in-house in R environment (https://github.com/ppernot/SK-Ana). Unlike the routine application of the developed codes to spectro-kinetics matrices data — built by delay-varying

measurements —, the global matrices in this work were constructed from the spectra of different [Ca^{2+}] concentrations, measured at D = 25 ns. By this means, the problem can be recast into a decomposable form that emphasizes the bilinearity between Ca^{2+}-dependent concentration and spectral properties, as expressed in the following equation:

$$F(\lambda, [Ca]) = \sum_{k} F_k(\lambda) C_k([Ca]) \quad (17)$$

where $F(\lambda, [Ca])$ (luminescent intensity), represents an additive result of pure spectral components $F_k(\lambda)$, of k principal components determined by SVD weighted by their concentration profile as a function of $C_k([Ca])$. This interpretation of luminescent spectra evolution is also chemically meaningful. However, it was noted in Ruckebusch *et al.* [56] that SVD can suffer from an excess of estimated rank towards the expected number of components when the pure spectral component of a single chemical compound shows a clear spectral shift, thus the sequential transformation of discrete components was applied in the decomposition in order to verify the concentration-wavelength separability [59].

The global matrices data analysis was conducted for the Ca series at 50°C. The first spectrum at [Ca^{2+}] = 0 was separately implemented as an external file serving as the reference shape, which can facilitate the calculation and improve the accuracy. The SVD analysis and the sequential transformation were tested for determining the number of components. The spectral intensity and concentration profiles of the components were constrained to be positive. It was shown by both methods that there are two distinguishable components, which is consistent with the hypothesis of $CaUO_2(CO_3)_3^{2-}$ and $Ca_2UO_2(CO_3)_3(aq)$ occurrences. The MCR-ALS analysis with two species results in a lack-of-fit (LOF) of 3.73%. The recovered spectra of $CaUO_2(CO_3)_3^{2-}$ and $Ca_2UO_2(CO_3)_3(aq)$ are shown in Fig. 5, compared to the experimentally acquired $UO_2(CO_3)_3^{4-}$ spectrum, see Fig S2 of the ESI for spectral decomposition. The spectrum decomposition was performed by fitting the emission bands into Gaussian-peak shape using Levenberg-Marquardt

method to evaluate the uncertainties — for details of decomposition information, see Table S9 of the ESI.

One can observe that at 50°C, the energy losses in luminescence are intensified for the incomplete complexations, *i.e.*, $UO_2(CO_3)_3^{4-}$ and $CaUO_2(CO_3)_3^{2-}$, that contribute to the red-shifted and strongly deformed spectra. On the contrary, the neutral charged species $Ca_2UO_2(CO_3)_3(aq)$ is more resistant to the temperature effect. The characteristic band positions were determined at 465, 484, 505, 526, and 549 nm for $Ca_2UO_2(CO_3)_3(aq)$ that are consistent with our previous results [34-35], whereas the pure spectral component of $CaUO_2(CO_3)_3^{2-}$ at 50°C exhibited obvious red-shifts with bands resolved at 480, 497, 515, 533, and 552 nm. The recovered spectra using the MCR-ALS analysis of $Ca_nUO_2(CO_3)_3^{(4-2n)-}$ at 40 and 45°C are not shown, but the trends in the spectral features are similar. The same procedure was also applied to the Mg-series at 30°C. As shown in Fig. S3 of the ESI, the pure spectral component of $MgUO_2(CO_3)_3^{2-}$ at 30°C did not show a shift compared to our previous measurements [36], with band positions determined at 466, 485, 503, 523, and 546 nm. It is believed that the spectral properties of Mg/Ca-UO_2-CO_3 complexes reflect subtle differences in the coordination of alkaline metal ion to triscarbonatouranyl(VI), which also affect their thermodynamic properties. This will be pointed out with the analysis of their thermodynamic functions in the following section.

Evaluation of equilibrium constants at different temperatures.

The graphical representations of linear regression results at different temperatures are shown in Fig. 6 for $Ca_nUO_2(CO_3)_3^{(4-2n)-}$ and in Fig. 7 for $MgUO_2(CO_3)^{2-}$. The stability constants at 22°C of $M_nUO_2(CO_3)_3^{(4-2n)-}$ had been measured during our previous studies [34,36]. The 2σ error bars are too small to be presented due to the trapezoidal integration method used to deduce the value of FI_0 (the fluorescence intensity at D = 0). Linear fits were achieved by weighted least-squares regression analysis with estimated parameters of slope and intercept mean values with 95% uncertainties. After rounding off the slope values to the integers of 1 and 2, *i.e.* the

stoichiometry of coordinated Mg^{2+}/Ca^{2+}, we obtained the conditional formation constants of $M_nUO_2(CO_3)_3^{(4-2n)-}$ listed in Table. 1 with the $\log_{10}K°_{n.1.3}$ extrapolated to infinite dilution by SIT.

Determination of enthalpy and entropy

The enthalpy of the formation of $M_nUO_2(CO_3)_3^{(4-2n)-}$ is the net thermal effect of three processes: i) the energy required for dehydration of Mg^{2+}/Ca^{2+} and $UO_2(CO_3)_3^{4-}$; ii) the energy released/required during the formation of $M_nUO_2(CO_3)_3^{(4-2n)-}$; and iii) the energy released/required during the formation of hydrogen bonding between the first inner-sphere water molecules and the surrounding bulk water. The value of $\Delta_r H°_m$ is established by the competition between the energy-consuming and -generating processes in complexation and a net gain/loss in energy balance resulting in negative/positive value of $\Delta_r H°_m$, respectively. The stability constants of $M_nUO_2(CO_3)_3^{(4-2n)-}$ determined in this work did not show obvious variation in the investigated temperature range that made the model parameters sensible to adjustment and resulted in large errors. Four approximation approaches were tested to fit the experimental $\log_{10}K°_{n.1.3}$: the Van't Hoff equation, the constant heat capacity equation, the DQUANT equation, and the isoelectric modification. Notwithstanding the different assumptions of each estimated model, as well as their corresponding temperature range of validity, the four approximation approaches provide satisfactory fitting of experimental data and allow prediction of the formation constants with temperatures. It must be reminded here that two digits will be kept for thermodynamic constants and entropy values, and three digits will be kept in the values of the Gibbs energy and enthalpy values, in coherence with the selected data of the NEA-TDB [37-39], even if they may not be significant.

With the values of $\log_{10}K°_{n.1.3}$ and $\Delta_r H°_m$ determined at 25°C using different approximation approaches, the temperature effect can be quantitatively estimated to predict the formation constants as a function of temperature. Fig. 8 shows that the approaches, including the Van't Hoff equation, the constant heat capacity equation, the DQUANT approach, and the isoelectric

modification method, provide satisfactory description of the measured $\log_{10}K°_{n.1.3}$ in the temperature ranges of 5-30°C for $MgUO_2(CO_3)_3^{2-}$ and 10-50°C for $Ca_nUO_2(CO_3)_3^{(4-2n)-}$. However, deviations start to increase at elevated temperature, *i.e.*, 70-90°C, reaching several logarithm units, especially between the values evaluated by the Van't Hoff equation and the constant heat capacity equation. Fig. 9 presents the variation of $\log_{10}K°_{n.1.3}$ uncertainties bands with temperature using the Van't Hoff approach.

As shown in Table. 2, the enthalpies were calculated by the Van't Hoff equation to be $\Delta_r^{VH}H°_m$ = (4.882 ± 5.949) kJ mol^{-1} and -(1.347 ± 11.879) kJ mol^{-1} for $CaUO_2(CO_3)_3^{2-}$ and $Ca_2UO_2(CO_3)_3$(aq), respectively, indicating that the first complexation of Ca^{2+} to $UO_2(CO_3)_3^{4-}$ is slightly endothermic. Similar values were obtained with the DQUANT equation, $\Delta_r^{DQUANT}H°_m$ = (4.306 ± 5.599) and -(2.134 ± 11.405) kJ mol^{-1} for $CaUO_2(CO_3)_3^{2-}$ and $Ca_2UO_2(CO_3)_3$(aq), respectively. However, the constant heat capacity model and the isoelectric modification approach suggested slightly exothermic reaction for the formation of $CaUO_2(CO_3)_3^{2-}$ with $\Delta_r^{CHC}H°_m$ = -(1.784 ± 6.145) kJ mol^{-1} and $\Delta_r^{Exo}H°_m$ = -(5.001 ± 5.395) kJ mol^{-1}, and for $Ca_2UO_2(CO_3)_3$(aq) with $\Delta_r^{CHC}H°_m$ = -(10.992 ± 14.150) kJ mol^{-1} and $\Delta_r^{Exo}H°_m$ = -(16.209 ± 9.064) kJ mol^{-1}. We specifically calculated the thermodynamic constants for the successive complexation of Ca^{2+} to $CaUO_2(CO_3)_3^{2-}$ by subtracting the values determined for $CaUO_2(CO_3)_3^{2-}$ from those for $Ca_2UO_2(CO_3)_3$(aq) (Table. 2). The uncertainties were apparently too large, due to the very weak variation of the values of $\log_{10}K°_{n.1.3}$ in the investigated temperature ranges.

One can note that for the formation of $CaUO_2(CO_3)_3^{2-}$, the entropy term $T\Delta_rS°_m$ varies from (27.79 ± 5.40) kJ mol^{-1} to (36.45 ± 5.96) kJ mol^{-1} at room temperature depending on the fitting equation. It seems though that the formation of $CaUO_2(CO_3)_3^{2-}$ is entropy-driven, consistent with the trends observed both by Endrizzi & Rao [18] and Jo *et al.* [28], whilst the enthalpy value is closely related to the approximation approach. In comparison, the second complexation of $CaUO_2(CO_3)_3^{2-}$ by Ca^{2+} is always exothermic regardless of the approximation approach. The

entropy term $T\Delta_r S°_m$ of this reaction — from (9.60 ± 10.56) kJ mol^{-1} to (13.80 ± 13.30) kJ mol^{-1} — shares nearly equal importance with the enthalpy term but is much less important than in the first complexation.

The decrease in entropy term for the first and second stepwise reactions may results principally from the degree of solvation and the polarity of surrounding water molecules of the reacting species and the complexes. The hydration shell of $UO_2(CO_3)_3^{4-}$ — highly charged and symmetric in structure — is much more ordered than that of the globally -2 bearing charge ion $CaUO_2(CO_3)_3^{2-}$. In the process of complexation, the ordered water molecules around $UO_2(CO_3)_3^{4-}$ have to be released to a disordered bulk solvent that allows a bidentate binding configuration for calcium. Therefore, the initial hydration shell of $UO_2(CO_3)_3^{4-}$ is inevitably perturbed by the first complexation, which explained the great entropy gain as a result of a large change in hydration sphere. The molecular calculations showed that the triscarbonatouranyl(VI) group can impose a specific geometry on the primary hydration sphere of calcium ion by reducing its coordination number from 7 to 5 [60]. In this respect, the second complexation of Ca^{2+} to $CaUO_2(CO_3)_3^{2-}$ should be less favourable in terms of entropy because the distorted hydration shell of $CaUO_2(CO_3)_3^{2-}$ may be easier to accept the next Ca^{2+} than the first one, which would result in a lower entropy gain [61]. In addition, it was postulated in classical molecular dynamics simulations [62] that the presence of solvent ion Na^+ is able to distort one of the three equatorial carbonate groups in $CaUO_2(CO_3)_3^{2-}$ from bidentate to monodentate, while the second Ca^{2+} is able to stabilize the bidentate binding of the three CO_3^{2-} in $Ca_2UO_2(CO_3)_3(aq)$. This conversion of denticity during the second complexation of $CaUO_2(CO_3)_3^{2-}$ by Ca^{2+} could partially contribute to an exothermic process due to the bond formation of $U\text{-}O_{CO_3}$, and a less important entropy value due to the formation of more ordered $Ca_2UO_2(CO_3)_3(aq)$, which agrees with our experimental results.

The reaction enthalpy and entropy values were determined for the formation of $MgUO_2(CO_3)_3^{2-}$ from the variation of stability constants in temperature range of 5-30°C with the four approximation approaches. The fitting results of the Van't Hoff equation and the DQUANT equation are of equal magnitude with slightly negative $\Delta_r^{VH}H°_m$ = -(11.653 ± 10.300) kJ mol^{-1} and $\Delta_r^{DQUANT}H°_m$ = -(11.171 ± 10.683) kJ mol^{-1}, while the constant heat capacity equation and isoelectric modification result in more exothermic process with $\Delta_r^{CHC}H°_m$ = -(13.477 ± 30.494) kJ mol^{-1} and $\Delta_r^{Iso}H°_m$ = -(12.025 ± 435) kJ mol^{-1}. In view of the high uncertainties, the enthalpy contribution to the formation of $MgUO_2(CO_3)_3^{2-}$ and $CaUO_2(CO_3)_3^{2-}$ may be both assumed to be almost nil. Our results are approximately consistent with the value directly measured at 25°C as $\Delta_r H°_m$ = (4.3 ± 1.5) kJ mol^{-1} using calorimetry by Jo *et al.* [29] It can be concluded that the entropy term contributes primarily to this reaction. However, unlike the comparable values of entropy term obtained for the formations of $MgUO_2(CO_3)_3^{2-}$ and $CaUO_2(CO_3)_3^{2-}$ in the work of Jo *et al.* [28-29] the value of $T\Delta_r S°_m$ determined in this study for the complexation of Mg^{2+} is globally lower than that of Ca^{2+} by about 10-20 kJ mol^{-1}. The decrease in entropy value from $CaUO_2(CO_3)_3^{2-}$ to $MgUO_2(CO_3)_3^{2-}$ might very well be attributed to the more ordered bulk water structure of $MgUO_2(CO_3)_3^{2-}$, which would also explain the lower $\log_{10}K°_{1.1.3}$ value for the complexation of Mg^{2+} compared to Ca^{2+}. Because of its higher charge density, Mg^{2+} — charge denticity of 205 C mm^{-3} calculated from $ne/(4/3)\pi r^3$ with e = 1.60 10^{-19} C, IR_{VI} = 0.72 Å in Shannon [63] assuming Mg^{2+} six-coordinated by H_2O — exhibits a stronger polarizing effect than Ca^{2+} — charge denticity of 64 C mm^{-3} with IR_{VII} = 1.06 Å in Shannon [63] assuming Ca^{2+} seven-coordinated by H_2O — in aqueous solution. When complexing to large negative ion like $UO_2(CO_3)_3^{4-}$ the smaller Mg^{2+} should distort the electron cloud of $UO_2(CO_3)_3^{4-}$ to a larger degree, and even could favour partial covalence between Mg and O_{CO_3}, which leads to a more consequent deformation of originally symmetric structure of $UO_2(CO_3)_3^{4-}$. Therefore, $MgUO_2(CO_3)_3^{2-}$ should be less symmetric in electron distribution and exhibits stronger polarizing power than

$CaUO_2(CO_3)_3^{2-}$ resulting in more ordered surrounding hydration sphere. This is in general agreement with the Hofmeister series, and kosmotrope character of Mg^{2+} relative to Ca^{2+} [64]. This subtle difference was detected in TRLFS using a more dispersing 1800 lines mm^{-1} grating [36,53].

Discrepancies in enthalpies depend on numerous factors: experimental technique, approximation approach, and the inherent weakness of magnesium/calcium tricarbonatouranyl complexation, which gives rise to difficulties in measurements. Those factors finally render it difficult to accurately determine the enthalpy and yield a large scatter in results. Direct measurements of enthalpy by microcalorimetry could theoretically carry out more accurate data than the slope analysis and help explaining the observed discrepancy. Nonetheless, this method suffers from the fact that the uranium concentration should be high enough to detect any heat flow in the titration chamber of the microcalorimeter. This constraint on uranium concentration hinders its application to high temperatures because such conditions, *i.e.*, concentrated uranium at elevated temperature, are much favourable to the formation of U(VI) polynuclear species, e.g., $(UO_2)_2CO_3(OH)_3^-$, due to the decrease of dielectric constant of water. Alternatively, the capabilities of TRLFS, especially in speciation measurements, show interest in probing luminescent $M_nUO_2(CO_3)_3^{(4-2n)-}$ complexes. The identification of each species based on spectroscopic fingerprints gives more confidence in the stoichiometry of Mg and Ca and thermodynamic constants and functions.

Practical applications

Case of nuclear waste repositories

The Boom clay and the Callovo-Oxfordian (COx) clay, identified as high-level long-lived radioactive waste repositories in Belgium and France [65-66], respectively, had been characterized with the chemical compositions of equilibrium waters given in de Craen *et al*. [9] and in Gaucher *et al*. [11] In our previous calculations using the experimentally determined

constants $\log_{10}K^{\circ}_{n.1.3}$ and ε at near standard conditions [34,36], it has been concluded that the high carbonate concentration in the Mol reference water in the Boom clay contributes to the formation of $M_nUO_2(CO_3)_3^{(4-2n)-}$ at 25°C, though U(IV) should dominate the solubility and control the mobility of uranium because of the reducing redox potential (E_h = -274 mV, or $P(O_2)= 10^{-68.67}$ atm) [67-69]. In the case of the COx equilibrium water — the solution A in Gaucher *et al.* [11]. of less reducing conditions than the Boom clay water (Eh = -163 mV, or $P(O_2)= 10^{-65.83}$ atm) —, the high calcium concentration ensures the predominance of the triscarbonatouranyl(VI) complexes, *i.e.*, $UO_2(CO_3)_3^{4-}$, $CaUO_2(CO_3)_3^{2-}$, only in neutral pH range at 25°C. At pH values higher than 8.5 the solution should be dominated by $U(OH)_4(aq)$ due to the lower carbonate concentrations — see Fig. 13 in Reiller & Descostes [20].

In nuclear waste management, the high-level waste (HLW) package disposal facilities are composed of multiple barriers to prevent the leaching of radionuclides from the stainless steel canisters (the primary barrier) and their contact with interstitial water. Theoretically, the thick steel overpacks wrapping the canister can protect the vitrified HLW from water corrosion for 500 years. Once the HLW packages are in underground repositories, the temperature of the cell can reach around 80°C in 10-15 years due to the generated heat by radioactive decay, but the temperature between two HLW cells needs a longer period to reach the peak, *e.g.*, 40-60°C after approximately 400-500 years dependent on the types of geological formation and waste [4].

To predict the uranium behaviour under repository conditions at temperatures higher than 25°C, the thermodynamic calculations were performed to determine the uranium speciation and to identify the mineral phases likely to precipitate using Thermochimie 10a database file [70], in which the uranium chemistry is largely based on NEA-OECD analyses [37-39]. The thermodynamic parameters for the interactions of UO_2-CO_3 with Mg/Ca were based on the isoelectric reaction approximation because of its higher validity range of temperature that would render more reliable estimates. The thermodynamic parameters in the form of analytical

expression to implement in the input PhreeqC file are listed in Table. 3. We noted that the determined values of $\log_{10}K°$ are so sensitive to the parameters in analytical expression that they should not be rounded off in calculation.

Water compositions in the Boom and COx geological formations were taken from de Craen, *et al*. [9] and Gaucher *et al*. [11] The aqueous uranium concentration was set in equilibrium with the dissolution of UO_2:$2H_2O$(am) phase in both calculations from Thermochimie 10a database file [70]— adapted from UO_2(am,hyd) in NEA-OECD analyses [38-39], in which the $\Delta_r H°_m$ value is absent. Fig. 10 shows the uranium solubility (Fig. 10a) and speciation (Fig. 10b) as a function of temperature for the Mol reference water. One can observe that the aqueous system undergoes a fast alteration of dominant species in the narrow temperature range of 40-50°C while the total uranium, majorly in U(VI) from 5°C to 50°C, suffers a steep decline then an increase controlled by U(IV) in the form of $U(OH)_4$(aq) at T > 50°C. As shown in Fig S4 of the ESI, the conversion of main oxidation states of Fe, S, C, and U suggests that the reducing conditions in the Boom clay at T > 50°C could be influenced by CH_4.

The uranium speciation and solubility in the COx solution also show sensible variations with response to temperature. As shown in Fig. 11a and b, $Ca_nUO_2(CO_3)_3^{(4-2n)-}$ complexes are dominant below 40°C with $Ca_2UO_2(CO_3)_3$(aq) about three times more than $CaUO_2(CO_3)_3^{2-}$. $U(OH)_4$(aq) becomes the only aqueous uranium species at 40°C. As temperature increases, the redox potential of water solution decreases further, which triggers the reduction of S(+VI) (mainly SO_4^{2-}) to S(-II) (mainly HS^-) and the precipitation of pyrite (FeS_2), and also the reduction of C(+IV) (mainly HCO_3^-) to C(-IV) (mainly CH_4(aq)). These processes are consuming protons, which eventually leads to an important increase of the pH value. Fig. S5 of the ESI displays the reduction of main oxidation states of Fe, S, C, and U, and the evolutions of pe and pH as a function of temperature. Due to the highly enriched sulphur quantity in COx in comparison to Mol reference water, the rapid increase of pH value up to 11.2 above 40°C mainly accounts for the

emergence of $UO_2(OH)_3^-$ over a narrow temperature range. At the same time, Fe(II)/Fe(III) oxidation is facilitated during this short oxidizing period. When T > 70°C, the redox potential is low due to the high temperature and reduction of S and C. The sample solution only contains $U(OH)_4(aq)$ as uranium species, which is consistent with the fact that the dipole moment of water decreases with increasing temperature and favours low or no charge species as the hydrogen bonding network weakens significantly. As the COx water is enriched in sulphur, the same calculation but without sulphur was performed in order to highlight the impacts of S(+VI)/S(-II) reduction by preventing all the unwanted S(+VI) reduction to lower oxidation states in initial input PhreeqC file. As shown in Fig. S6b of the ESI, the crossing point of $Ca_2UO_2(CO_3)_3(aq)$ and $U(OH)_4(aq)$ curves occurred *ca.* 60°C, compared to *ca*. 42°C in Fig. 11b with sulphur in solution. The peak of pH value without sulphur in solution was reduced to 9.10 (Fig. S6d of the ESI) instead of 11.2 (Fig. S5b) due to the lack of S(+VI)/S(-II) reduction. The predominance of $U(OH)_4(aq)$ is maintained until 90°C and excluded the perturbation of $UO_2(OH)_3^-$.

Hence, the formation of $U(OH)_4(aq)$ may thus play an important role in reduced uranium transport. At 40-60°C, our simulation results suggest that uranium would primarily exist in the reduced state in the form of $U(OH)_4(aq)$ in the COx and Mol waters and the stability of UO_2 can be sustained by the presence of pyrite (FeS_2), which consumes the oxygen supplied by infiltrating water [71]. In the very long term, the temperature in the near field of the repository will decrease to ambient temperature [4]. As hard-soft-acid-base principles suggested, the uranyl ion, a hard (high charge to radius ratio) cation, should form strong complexes with carbonate ions, which are hard anions. Thus the uranium migration would be promoted because of $Ca_nUO_2(CO_3)_3^{(4-2n)-}$ predominance in the COx and Mol waters as suggested by previous calculations [34-36].

Furthermore, one can note that the variation of uranium solubility as a function of temperature depends on the chosen solubility controlling phase in calculation. There is an underlying assumption in HLW management that reducing conditions will prevent uranium migration due to the formation of uranium ore deposits [72-78]. The principal ore minerals includes two main types — uraninite and pitchblende, both nominally UO_2 — that differ from each other in their depositional setting and chemical constitution [79-81]. As no value of enthalpy for $UO_2{:}2H_2O(am)$ selected either in the NEA-OECD analyses [38-39], or Thermochimie 10a database file, special focus was put on the Mol and COx water systems in equilibrium with the dissolution of uraninite $UO_2(cr)$ for which the $\Delta_r H°_m$ value is available. Fig. S7 of the ESI shows the solubility variation of $UO_2(cr)$ as a function of temperature for Mol and COx waters. Compared with Fig. 10a and 11a, one can observe that the uranium concentration in solution is lowered by about 10 orders of magnitude in both cases. In equilibrium with $UO_2(cr)$, the reduction of U(VI) to U(IV) is more intensely affected by temperature, as evidenced stronger decrease of the dissolved uranium concentration.

Conclusions

The present study reports the formation constants for the complexation of triscarbonatouranyl(VI) with Mg^{2+}/Ca^{2+} in 5-30°C for $MgUO_2(CO_3)_3^{2-}$ and 10-50°C for $Ca_nUO_2(CO_3)_3^{(4-2n)-}$ measured by TRLFS. The variation of $\log_{10}K°_{n.1.3}$ with temperature were fitted by several theoretical approaches: the Van't Hoff equation, the constant heat capacity model, the DQUANT equation, and the isoelectric reaction modification. In the experimental temperature ranges, these approximation models provided satisfactory matching between the experimentally derived constants and the predicted values. Nonetheless, large discrepancy has been observed between the predictions of $\log_{10}K°_{n.1.3}$ by the revised approaches, probably because of the narrow experimental temperature ranges that were limited by the quenching effects with temperature. The Van't Hoff equation and the DQUANT equation showed comparable trends of $\log_{10}K°_{n.1.3}$, while the assumption of non-zero heat capacity resulted in significant deviation at high temperatures. The modification to isoelectric reaction exhibited mildly increasing $\log_{10}K°_{n.1.3}$ with temperature. The accuracy of the experimental values of equilibrium constants at elevated temperatures for these species should be improved by further investigations. The recent thermodynamic data with response to temperature and ionic strength for $M_nUO_2(CO_3)_3^{(4-2n)-}$ complexes are highly valuable in estimating the temperature and salinity effects on the speciation of U(VI), especially encountered in nuclear waste repositories and bridging the gaps in the thermodynamic database for the proposed important $M_nUO_2(CO_3)_3^{(4-2n)-}$ complexes.

Funding sources

This work was financed by ONDRAF-NIRAS (contract DEN4857-CCHO 2018-0456/00/00).

Conflicts of Interest

There are no conflicts to declare.

Acknowledgment. The authors thank Dr. Pascal Pernot, who developed the MCR-ALS analysis code in the R environment, for his help; and Dr. Hélène Isnard who prepared the uranium(VI) solution.

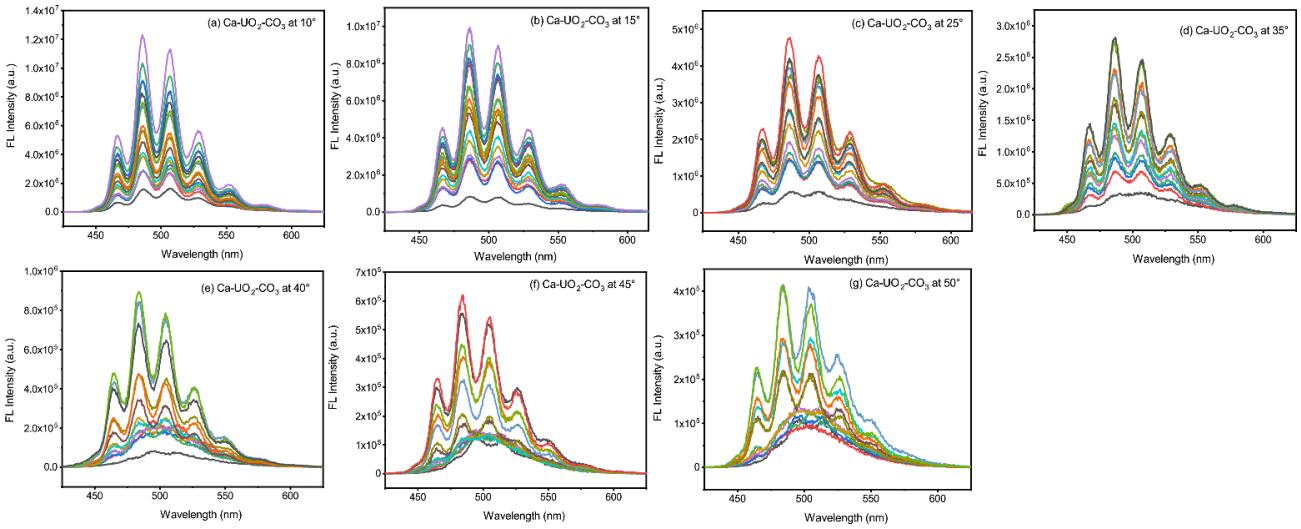

Fig. 1. Evolution of luminescence emission spectra during complexation of Ca(II) with $UO_2(CO_3)_3^{4-}$ at different temperature (a)-(f): 10-50°C. The experimental conditions for prepared samples listed in Table S5.

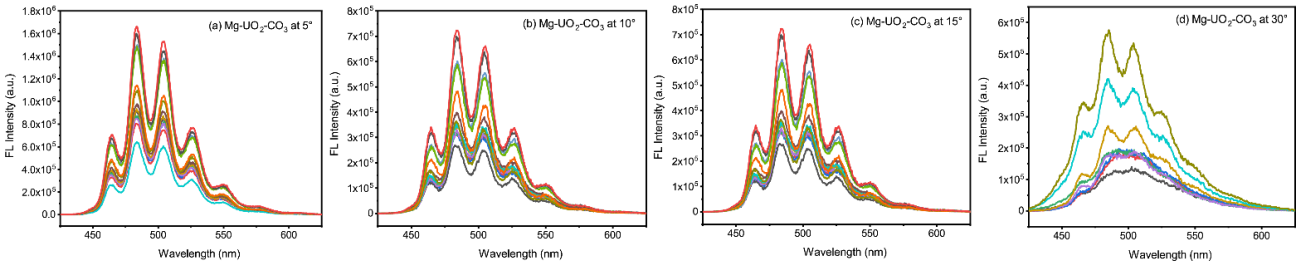

Fig. 2 Evolution of luminescence emission spectra during complexation of Mg(II) with $UO_2(CO_3)_3^{4-}$ at different temperature (a)-(d): 5-30°C. The experimental conditions for prepared samples listed in Table S5.

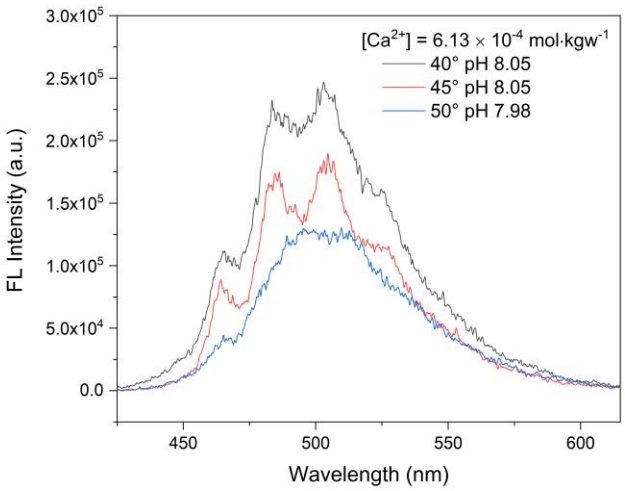

Fig. 3 Luminescence emission spectra at higher temperatures than the ambient of the sample: [U(VI)] = 50 µm, $[Ca^{2+}]$ = 6.13 10^{-4} mol kg_w^{-1}, pH ≈ 8 with the dominant species $CaUO_2(CO_3)_3^{2-}$ in solution.

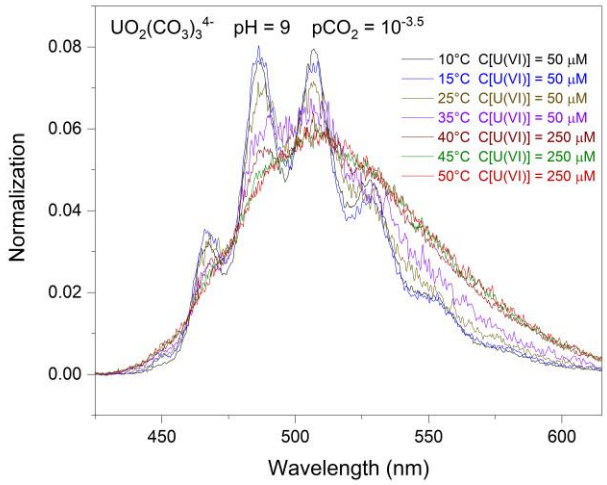

Fig. 4 Luminescence emission spectra of $UO_2(CO_3)_3^{4-}$ normalized to the same area at *D* = 25 ns; the concentration of [U(VI)] increased at high temperatures (40-50°C) to enhance the emission intensity.

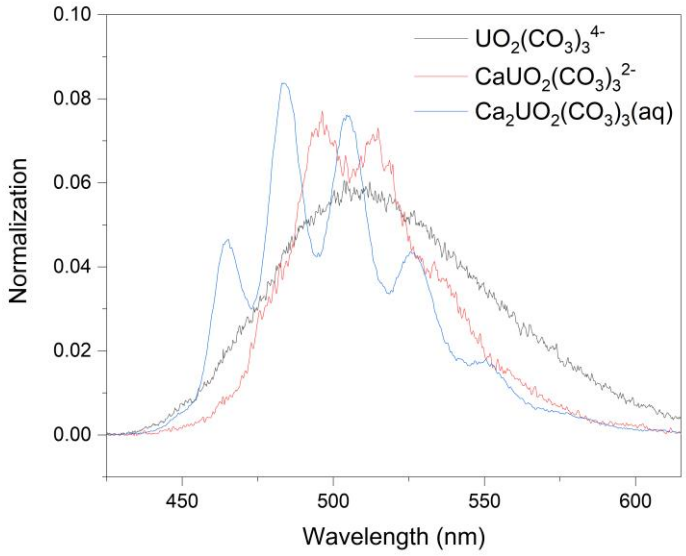

Fig. 5 Pure emission spectral component obtained from MCR-ALS analysis of the complexation of Ca^{2+} with $UO_2(CO_3)_3^{4-}$ at 50°C.

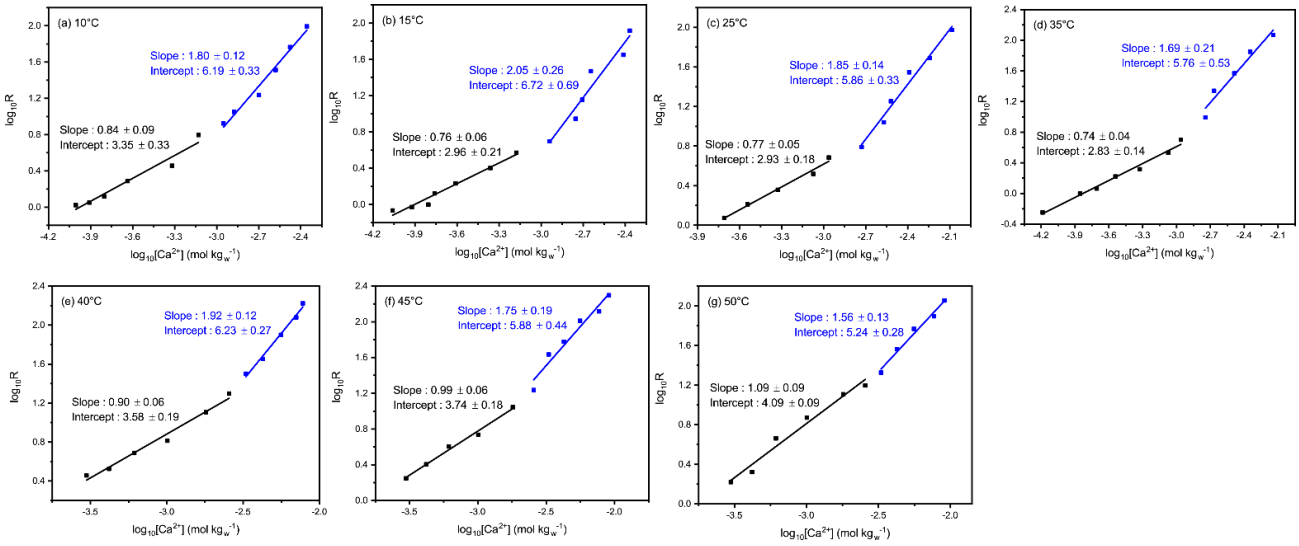

Fig. 6 Plot of logarithm ratio of R as a function of $\log_{10}[Ca^{2+}]$ (m) at (a)-(f): 10-50°C: $[U]_{total}$ = 50 µm.

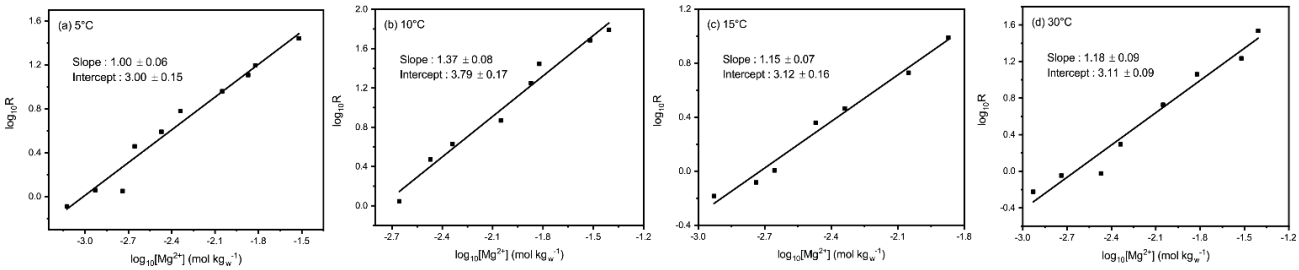

Fig. 7 Plot of logarithm ratio of R as a function of $\log_{10}[Mg^{2+}]$ (m) at (a)-(d): 5-30°C: $[U]_{total}$ = 50 µm.

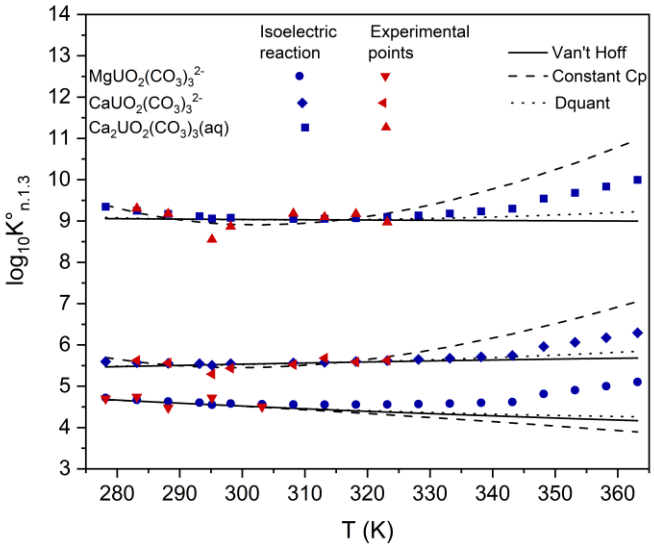

Fig. 8 Dependence on temperature of the thermodynamic constants for $M_nUO_2(CO_3)_3^{(4-2n)-}$ with lines: the fitted curves based on the Van't Hoff equation, the constant heat capacity equation and the DQUANT equation and red points: the values of $\log_{10}K°_{n.1.3}$ recalculated for each temperature with the isoelectric reaction, as listed in Table S7 of the ESI.

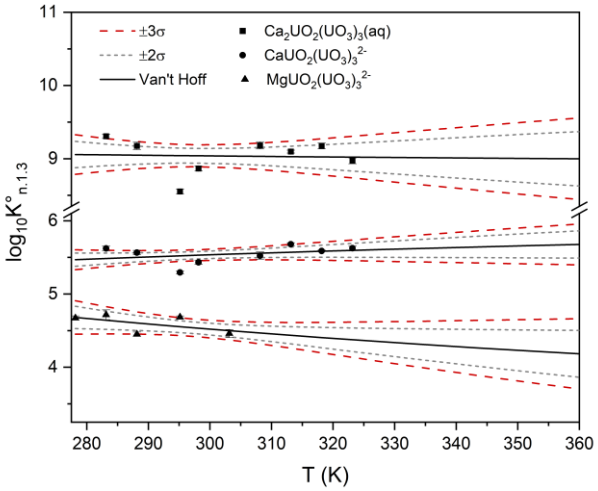

Fig. 9 Dependence on temperature of the thermodynamic constants for $Mg_nCa_nUO_2(CO_3)_3^{(4-2n)-}$ with lines represented fitted curves based on the Van't Hoff equation, grey short-dashed lines display the 95% confidence interval and red long-dashed lines show the 98% confidence level (see thermodynamic parameters in Table. 2).

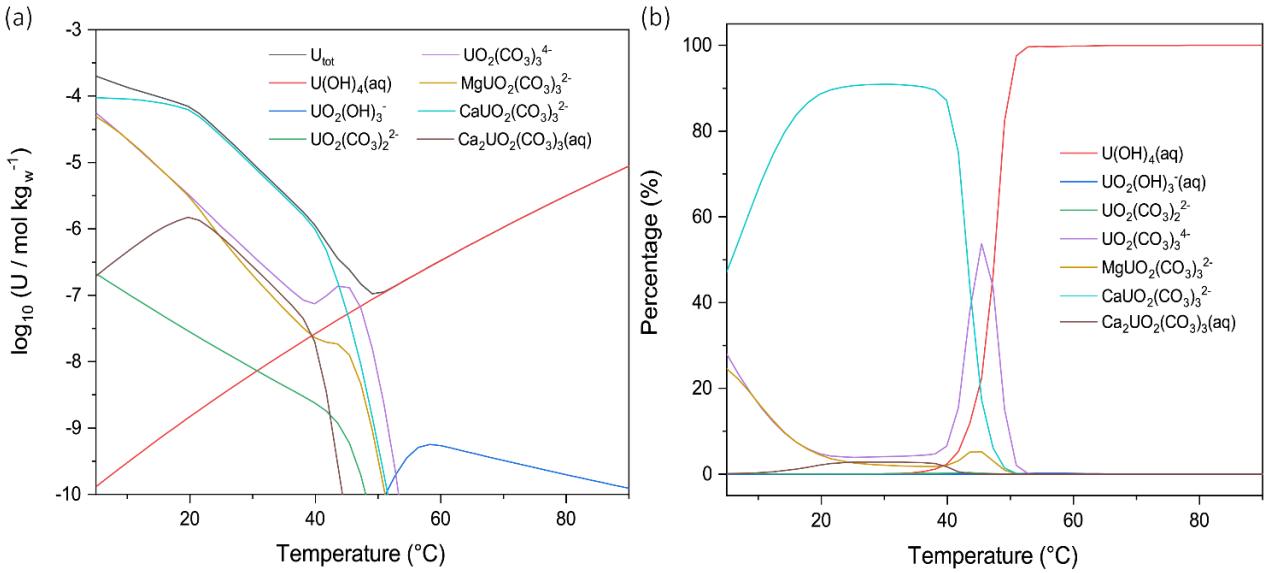

Fig. 10 Solubility of $UO_2{:}2H_2O$(am) (a) and aqueous uranium speciation (b) *vs.* temperature for Boom clay equilibrium water ($P(O_2) = 10^{-68.67}$ atm) using thermodynamic data from the Thermochimie 10a database,[70] implementing $SrUO_2(CO_3)_3^{2-}$,[26] specific ion interaction coefficients of $Mg_nCa_nUO_2(CO_3)_3^{(4-2n)-}$, [34-36] and their $\Delta_r H°_m$ values determined in this work based on the isoelectric reaction approximation.

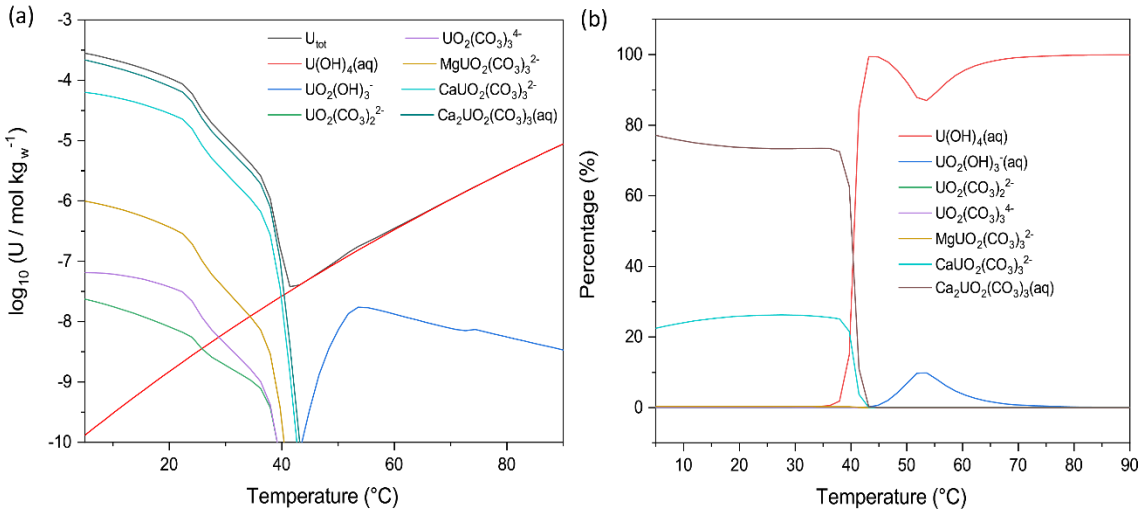

Fig. 11 Solubility of $UO_2{:}2H_2O$(am) (a) and aqueous uranium speciation (b) as a function of temperature for Callovo-Oxfordian clay equilibrium waters[11] $P(O_2) = 10^{-65.83}$ atm using thermodynamic data from the Thermochimie 10a database,[70] implementing $SrUO_2(CO_3)_3^{2-}$,[26] specific ion interaction coefficients of $Mg_nCa_nUO_2(CO_3)_3^{(4-2n)-}$,[34-36] and their $\Delta_r H°_m$ values determined in this work based on the isoelectric reaction approximation.

Table. 1 Formation constants $\log_{10}K_{n.1.3}$ derived from the rounded off slopes in Fig. 6 and 7 with values of $\log_{10}K_{0.1.3}°$ taken from Götz *et al*.[50]

$Ca_nUO_2(CO_3)_3^{(4-2n)-}$

T (°C)	$\log_{10}K_{1.1.3}$	$\log_{10}K_{2.1.3}$	$\log_{10}K°_{1.1.3}$	$\log_{10}K°_{2.1.3}$	$\log_{10}K°_{0.1.3}$	$\log_{10}\beta°_{1.1.3}$	$\log_{10}\beta°_{2.1.3}$
10	3.92 ± 0.03	6.73 ± 0.03	5.62 ± 0.03	9.31± 0.03	22.28 ± 0.04	27.91 ± 0.04	31.59± 0.04
15	3.85 ± 0.03	6.58 ± 0.05	5.57 ± 0.03	9.17± 0.05	22.11 ± 0.04	27.68 ± 0.04	31.28± 0.05
22[34]	3.56 ± 0.02	5.93 ± 0.03	5.29 ± 0.02	8.55± 0.03	21.93 ± 0.04	27.22 ± 0.04	30.48± 0.05
25	3.69 ± 0.03	6.23 ± 0.03	5.43 ± 0.03	8.87± 0.03	21.81 ± 0.04	27.24 ± 0.04	30.68± 0.04
35	3.75 ± 0.05	6.52 ± 0.05	5.52 ± 0.05	9.18± 0.05	21.58 ± 0.04	27.10 ± 0.05	30.76 ± 0.04
40	3.89 ± 0.02	6.41 ± 0.02	5.68 ± 0.02	9.10± 0.02	21.48 ± 0.04	27.16 ± 0.04	30.58± 0.04
45	3.78 ± 0.01	6.46 ± 0.04	5.59 ± 0.01	9.17± 0.04	21.40 ± 0.04	26.99 ± 0.04	30.57± 0.04
50	3.80 ± 0.03	6.23 ± 0.04	5.63 ± 0.03	8.97± 0.04	21.33 ± 0.04	26.96 ± 0.04	30.30± 0.04

$MgUO_2(CO_3)_3^{2-}$

T (°C)	$\log_{10}K_{1.1.3}$	$\log_{10}K°_{1.1.3}$	$\log_{10}K°_{0.1.3}$	$\log_{10}\beta°_{1.1.3}$
5	3.00 ± 0.03	4.67 ± 0.03	22.48 ± 0.04	27.18 ± 0.04
10	3.04 ± 0.07	4.72 ± 0.07	22.28 ± 0.04	27.03 ± 0.07
15	2.76 ± 0.03	4.45 ± 0.03	22.11 ± 0.04	26.59 ± 0.04
22[36]	2.98 ± 0.02	4.68 ± 0.02	21.93 ± 0.04	26.65 ± 0.04
30	2.73 ± 0.05	4.46 ± 0.05	21.69 ± 0.04	26.32 ± 0.05

Table. 2 Comparison of thermodynamic parameters for the formations of $M_nUO_2(CO_3)_3^{(4-2n)-}$ obtained by different approximation approaches.

	Model	$\log_{10}K°_{n.1.3}$ ± 2σ at 25°C	$\log_{10}\beta°_{n.1.3}$ ± 2σ at 25°C	$\Delta_rH°_m$ ± 2σ (kJ mol^{-1}) at 25°C	$T\Delta_rS°_m$ ± 2σ (kJ mol^{-1}) at 25°C
	[a] $Ca^{2+} + UO_2(CO_3)_3^{4-} = CaUO_2(CO_3)_3^{2-}$				
Ca(II)	Van't Hoff	5.53 ± 0.05	27.37 ± 0.06	4.882 ± 5.949	36.45 ± 5.96
	$\Delta_r^{VH}G°_m$ = -31.565 ± 0.285 kJ mol^{-1}				
	$\Delta_f^{VH}G°_m$ = -3 245.285 ± 4.550 kJ mol^{-1}				
	$\Delta_f^{VH}H°_m$ = -3 618.800 ± 7.484 kJ mol^{-1}				
	$^{VH}S°_f$ = 104.500 ± 24.663 J K^{-1} mol^{-1}				
	Constant C_p	5.45 ± 0.06	27.29 ± 0.07	-1.784 ± 6.145	29.32 ± 6.15
	$\Delta_rC°_{p.m}$ = 1.74 ± 0.93 kJ mol^{-1}				
	DQUANT	5.52 ± 1.38	27.36 ± 1.38	4.306 ± 5.599	35.81 ± 5.51
	Isoelectric	5.74 ± 0.05	27.58 ± 0.06	-5.001 ± 5.395	27.79 ± 5.40
	[b] $Ca^{2+} + CaUO_2(CO_3)_3^{2-} = Ca_2UO_2(CO_3)_3$				
	Van't Hoff	3.51 ± 0.11		-6.229 ± 13.285	13.80 ± 13.30
	$\Delta_r^{VH}G°_m$ = -572.842 ± 5.470 kJ mol^{-1}				
	Constant C_p	3.47 ± 0.15		-9.208 ± 15.427	10.60 ± 15.45
	$\Delta_rC°_{p.m}$ = 0.77 ± 2.33 kJ mol^{-1}				
	DQUANT	3.51 ± 3.12		-6.440 ± 12.705	13.61 ± 12.50
	Isoelectric	3.62 ± 0.09		-11.208 ± 10.548	9.60 ± 10.56
	[c] $2Ca^{2+} + UO_2(CO_3)_3^{4-} = Ca_2UO_2(CO_3)_3$				
	Van't Hoff	9.04 ± 0.10	30.88 ± 0.11	-1.347 ± 11.879	50.25 ± 11.89
	$\Delta_r^{VH}G°_m$ = -51.601 ± 0.571 kJ mol^{-1}				
	$\Delta_f^{VH}G°_m$ = -3 818.127 ± 3.035 kJ mol^{-1}				
	$\Delta_f^{VH}H°_m$ = -4 169.290 ± 12.835 kJ mol^{-1}				
	$^{VH}S°_f$ = 94.585 ± 42.450 J K^{-1} mol^{-1}				
	Constant C_p	8.92 ± 0.14	30.76 ± 0.15	-10.992 ± 14.150	39.92 ± 14.17
	$\Delta_rC°_{p.m}$ = 2.51 ± 2.14 kJ mol^{-1}				
	DQUANT	9.03 ± 2.80	30.87 ± 2.80	-2.134 ± 11.405	49.42 ± 11.22
	Isoelectric	9.39 ± 0.07	31.23 ± 0.08	-16.209 ± 9.064	37.39 ± 9.07
	[d] $Mg^{2+} + UO_2(CO_3)_3^{4-} = MgUO_2(CO_3)_3^{2-}$				
Mg(II)	Van't Hoff	4.53 ± 0.08	26.37 ± 0.09	-11.653 ± 10.300	14.22 ± 10.31
	$\Delta_r^{VH}G°_m$ = -25.876 ± 0.450 kJ mol^{-1}				
	$\Delta_f^{VH}G°_m$ = -3 142.170 ± 2.542 kJ mol^{-1}				
	$\Delta_f^{VH}H°_m$ = -3 562.540 ± 11.228 kJ mol^{-1}				
	$^{VH}S°_f$ = -50.859 ± 37.676 J K^{-1} mol^{-1}				
	Constant Cp	4.53 ± 0.10	26.37 ± 0.11	-13.477 ± 30.494	12.38 ± 30.50
	$\Delta_rC°_{p.m}$ = 0.224 ± 3.409 kJ mol^{-1}				
	DQUANT	4.53 ± 2.69	26.37 ± 2.69	-11.171 ± 10.683	14.70 ± 11.00
	Isoelectric	4.54 ± 0.09	26.38 ± 0.10	-12.025 ± 12.435	13.89 ± 12.45

Table. 3 Parameters in the expression of $\log_{10}K°_{n.1.3}(T) = A_1+A_2\ T+A_3\ T^{-1}+A_4\ \log_{10}T+A_5T^{-2}$ (T in Kelvin) based on the isoelectric reaction modification in Table. 1; the values of $\log_{10}K°_{n.1.3}$ at 70°C calculated by PhreeqC and used to perfom the uranium speciation, shown in Fig. 10.

Isoelectric reaction	**A_1**	**A_2**	**A_3**	**A_4**	**A_5**	**$\log_{10}K°_{n.1.3}$ at**
$CaUO_2(CO_3)_3^{2-}$	33822.8	6.01794	-1647050	-12537.7759	83260000	5.81
$Ca_2UO_2(CO_3)_3(aq)$	35198.8	6.25537	-1722880	-13040.2035	88090000	9.42
$MgUO_2(CO_3)_3^{2-}$	33994.3	6.04948	-1654900	-12602.4447	83660000	4.69

References

[1] Wronkiewicz D.J., Buck E.C. (2018) Uranium Mineralogy and the Geologic Disposal of Spent Nuclear Fuel (Peter C.B., Robert J.F., Eds.) Uranium Mineralogy and the Geologic Disposal of Spent Nuclear Fuel. De Gruyter. p. 475. https://doi.org/10.1515/9781501509193-015.

[2] Metz V., Geckeis H., González-Robles E., Loida A., Bube C., Kienzler B. (2012) Radionuclide behaviour in the near-field of a geological repository for spent nuclear fuel. *Radiochim. Acta* **100** 699.

[3] Rao L., Tian G., Xia Y., Friese J.I., Zanonato P., Di Bernardo P. (2010) Bridging the Gap in the Chemical Thermodynamic Database for Nuclear Waste Repository: Studies of the Effect of Temperature on Actinide Complexation (Wai C.M., Mincher B.J., Eds.) Nuclear Energy and the Environment. American Chemical Society. p. 299.

[4] Villar M.V., Armand G., Conil N., de Lesquen C., Herold P., Simo E., Mayor J.C., Dizier A., Li X., Chen G., Leupin O., Niskanen M., Bailey M., Thompson S., Svensson D., Sellin P., Hausmannova L. (2020) Initial SotA on THM Behaviour of I) Buffer Clay Materials and of II) Host Clay Materials. Deliverable D7.1 HITEC. EURAD Project. http://www.ejp-eurad.eu/publications/eurad-deliverable-71-initial-sota-thm-behaviour-i-buffer-clay-materials-and-ii-host.

[5] Marshall W.L., Franck E.U. (1981) Ion product of water substance, 0-1000°C, 1-10,000 bars New International Formulation and its background. *J. Phys. Chem. Ref. Data* **10** 295.

[6] Fernández D.P., Goodwin A., Lemmon E., Sengers J.L., Williams R.C. (1997) A Formulation for the Static Permittivity of Water and Steam at Temperatures from 238 K to 873 K at Pressures up to 1200 MPa, Including Derivatives and Deby… Hückel Coefficients. *J. Phys. Chem. Ref. Data* **26** 1125.

[7] Grenthe I., Puigdomenech I., Allard B. (1997) Modelling in Aquatic Chemistry. OECD Publishing, Issy-les-Moulineaux, France.

[8] Cao X., Zheng L., Hou D., Hu L. (2019) On the long-term migration of uranyl in bentonite barrier for high-level radioactive waste repositories: The effect of different host rocks. *Chem. Geol.* **525** 46.

[9] de Craen M., Wang L., Van Geet M., Moors H. (2004) Geochemistry of Boom Clay pore water at the Mol site. SCK•CEN, SCK•CEN-BLG-990. Mol, Belgium. http://jongeren.sckcen.be/~/media/Files/Science/disposal_radioactive_waste/Geochemistry_of_Boom_Clay_pore_Status_2004.pdf.

[10] Laaksoharju M., Smellie J., Tullborg E.-L., Gimeno M., Hallbeck L., Molinero J., Waber N. (2008) Bedrock hydrogeochemistry Forsmark - Site descriptive modelling SDM-Site Forsmark. SKB, R-08-47. Stockholm. http://www.skb.com/publication/1841127/R-08-47.pdf.

[11] Gaucher E.C., Tournassat C., Pearson F.J., Blanc P., Crouzet C., Lerouge C., Altmann S. (2009) A robust model for pore-water chemistry of clayrock. *Geochim. Cosmochim. Acta* **73** 6470.

[12] Fernández A.M., Cuevas J., Rivas P. (2011) Pore Water Chemistry of the Febex Bentonite. *MRS Proceedings* **663** 573. 573.

[13] Fernández A.M., Turrero M.J., Sánchez D.M., Yllera A., Melón A.M., Sánchez M., Peña J., Garralón A., Rivas P., Bossart P., Hernán P. (2007) On site measurements of the redox and carbonate system parameters in the low-permeability Opalinus Clay formation at the Mont Terri Rock Laboratory. *Phys. Chem. Earth* **32** 181.

[14] Cao X., Hu L., Wang J., Wang J. (2017) Radionuclide transport model for risk evaluation of high-level radioactive waste in Northwestern China. *Hum. Ecol. Risk Assess.* **23** 2017.

[15] Bernhard G., Geipel G., Brendler V., Nitsche H. (1996) Speciation of uranium in seepage waters of a mine tailing pile studied by time-resolved laser-induced fluorescence spectroscopy (TRLFS). *Radiochim. Acta* **74** 87.
[16] Tullborg E.L., Suksi J., Geipel G., Krall L., Auque L., Gimeno M., Puigdomènech I. (2017) The occurrences of $Ca_2UO_2(CO_3)_3$ complex in Fe(II) containing deep groundwater at Forsmark, eastern Sweden. *Proced. Earth Plan. Sci.* **17** 440.
[17] Prat O., Vercouter T., Ansoborlo E., Fichet P., Perret P., Kurttio P., Salonen L. (2009) Uranium speciation in drinking water from drilled wells in southern Finland and its potential links to health effects. *Environ. Sci. Technol.* **43** 3941.
[18] Endrizzi F., Rao L.F. (2014) Chemical speciation of uranium(VI) in marine environments: Complexation of calcium and magnesium ions with $[(UO_2)(CO_3)_3]^{4-}$ and the effect on the extraction of uranium from seawater. *Chem.-Eur. J.* **20** 14499.
[19] Maloubier M., Solari P.L., Moisy P., Monfort M., Den Auwer C., Moulin C. (2015) XAS and TRLIF spectroscopy of uranium and neptunium in seawater. *Dalton Trans.* **44** 5417.
[20] Reiller P.E., Descostes M. (2020) Development and application of the thermodynamic database PRODATA dedicated to the monitoring of mining activities from exploration to remediation. *Chemosphere* **251** 126301.
[21] Bernhard G., Geipel G., Reich T., Brendler V., Amayri S., Nitsche H. (2001) Uranyl(VI) carbonate complex formation: validation of the $Ca_2UO_2(CO_3)_3$(aq) species. *Radiochim. Acta* **89** 511.
[22] Lee J.Y., Vespa M., Gaona X., Dardenne K., Rothe J., Rabung T., Altmaier M., Yun J.-I. (2017) Formation, stability and structural characterization of ternary $MgUO_2(CO_3)_3^{2-}$ and $Mg_2UO_2(CO_3)_3$(aq) complexes. *Radiochim. Acta* **105** 171.
[23] Kalmykov S.N., Choppin G.R. (2000) Mixed $Ca^{2+}/UO_2^{2+}/CO_3^{2-}$ complex formation at different ionic strengths. *Radiochim. Acta* **88** 603.
[24] Geipel G., Amayri S., Bernhard G. (2008) Mixed complexes of alkaline earth uranyl carbonates: a laser-induced time-resolved fluorescence spectroscopic study. *Spectrochim. Acta, Part A* **71** 53.
[25] Götz C., Geipel G., Bernhard G. (2010) The influence of the temperature on the carbonate complexation of uranium(VI): a spectroscopic study. *J. Radioanal. Nucl. Chem.* **287** 961.
[26] Dong W., Brooks S.C. (2006) Determination of the formation constants of ternary complexes of uranyl and carbonate with alkaline earth metals (Mg^{2+}, Ca^{2+}, Sr^{2+}, and Ba^{2+}) using anion exchange method. *Environ. Sci. Technol.* **40** 4689.
[27] Dong W., Brooks S.C. (2008) Formation of aqueous $MgUO_2(CO_3)_3^{2-}$ complex and uranium anion exchange mechanism onto an exchange resin. *Environ. Sci. Technol.* **42** 1979.
[28] Jo Y., Kirishima A., Kimuro S., Kim H.-K., Yun J.-I. (2019) Formation of $CaUO_2(CO_3)_3^{2-}$ and $Ca_2UO_2(CO_3)_3$(aq) complexes at variable temperatures (10 – 70 °C). *Dalton Trans.* **48** 6942.
[29] Jo Y., Kim H.-K., Yun J.-I. (2019) Complexation of $UO_2(CO_3)_3^{4-}$ with Mg^{2+} at varying temperatures and its effect on U(VI) speciation in groundwater and seawater. *Dalton Trans.* **48** 14769.
[30] Kelly S.D., Kemner K.M., Brooks S.C. (2007) X-ray absorption spectroscopy identifies calcium-uranyl-carbonate complexes at environmental concentrations. *Geochim. Cosmochim. Acta* **71** 821.
[31] Amayri S., Reich T., Arnold T., Geipel G., Bernhard G. (2005) Spectroscopic characterization of alkaline earth uranyl carbonates. *J. Solid State Chem.* **178** 567.
[32] Tirler A.O., Hofer T.S. (2014) Structure and dynamics of the uranyl tricarbonate complex in aqueous solution: insights from quantum mechanical charge field molecular dynamics. *J. Phys. Chem. B* **118** 12938.
[33] Tirler A.O., Hofer T.S. (2016) The structural influence of Ca^{2+} counter ions on uranyl(VI) tricarbonate in aqueous solution. *Dalton Trans.* **45** 4983.

[34] Shang C., Reiller P.E. (2020) Determination of formation constants and specific ion interaction coefficients for $Ca_nUO_2(CO_3)_3^{(4-2n)-}$ complexes in NaCl solution by time-resolved laser-induced luminescence spectroscopy. *Dalton Trans.* **49** 466.

[35] Shang C., Reiller P.E., Vercouter T. (2020) Spectroluminescence measurements of stability constants of $Ca_nUO_2(CO_3)_3^{(4-2n)-}$ complexes in $NaClO_4$ medium and investigation of interaction effects. *Dalton Trans.* **49** 15443.

[36] Shang C., Reiller P. (2021) Thermodynamic constant of $MgUO_2(CO_3)_3^{2-}$ complex in $NaClO_4$ and NaCl media using time-resolved luminescence spectroscopy, and applications to different geochemical contexts. *Dalton Trans.* **50** 4363.

[37] Grenthe I., Fuger L., Konings R.G.M., Lemire R.J., Muller A.B., Nguyen-Trung C., Wanner H. (1992) Chemical Thermodynamics 1. Chemical Thermodynamics of Uranium. North Holland Elsevier Science Publishers B. V., Amsterdam, The Netherlands. http://www.oecd-nea.org/dbtdb/pubs/uranium.pdf.

[38] Guillaumont R., Fanghänel T., Neck V., Fuger J., Palmer D.A., Grenthe I., Rand M.H. (2003) Update of the Chemical Thermodynamics of Uranium, Neptunium, Plutonium, Americium and Technetium. OECD Nuclear Energy Agency, Data Bank, Issy-les-Moulineaux, France.

[39] Grenthe I., Gaona X., Plyasunov A.V., Rao L., Runde W.H., Grambow B., Koning R.J.M., Smith A.L., Moore E.E. (2020) Chemical Thermodynamics 14. Second Update on the Chemical Thermodynamics of Uranium, Neptunium, Plutonium, Americium and Technetium. OECD Nuclear Energy Agency Data Bank, Eds., OECD Publications, Paris, France. https://www.oecd-nea.org/jcms/pl_46643/second-update-of-u-np-pu-am-and-tc.

[40] Maia F.M.S., Ribet S., Bailly C., Grivé M., Madé B., Montavon G. (2021) Evaluation of thermodynamic data for aqueous Ca-U(VI)-CO_3 species under conditions characteristic of geological clay formation. *Appl. Geochem.* **124**. 104844.

[41] Plummer L.N., Busenberg E. (1982) The solubilities of calcite, aragonite and vaterite in CO_2-H_2O solutions between 0 and 90°C, and an evaluation of the aqueous model for the system $CaCO_3$-CO_2-H_2O. *Geochim. Cosmochim. Acta* **46** 1011.

[42] Robie R.A., Hemingway B.S. (1995) Thermodynamic Properties of Minerals and Related Substances at 298.15 K and 1 bar (10^5 Pascal) Pressure and at Higher Temperatures. US Geological Survey, US Geological Survey Bulletin, 2131. Denver, CO, USA. http://pubs.usgs.gov/bul/2131/report.pdf.

[43] Wu Y.C., Koch W.F., Durst R.A. (1988) Standardization of pH measurements. US Department. of Commerce, National Bureau of Standards, 260-53. http://nvlpubs.nist.gov/nistpubs/Legacy/SP/nbsspecialpublication260-53e1988.pdf.

[44] Fromentin E., Lebeau D., Bergounioux A., Ferry M., Reiller P.E. (2020) Complexation of Eu(III) by relevant hydro-soluble degradation products from a radio-oxidized polyesterurethane in contexts of repositories for low and intermediate level radioactive waste. *Radiochim. Acta* **108** 383.

[45] Ringböm A. (1963) Complexation in Analytical Chemistry: A Guide for the Critical Selection of Analytical Methods Based on Complexation Reactions. Interscience Publishers, New York, NY, USA.

[46] Giffaut E., Vitorge P., Capdevila H. (1993) Corrections de Température sur les Coefficients d'Activité Calculés selon la TIS. Commissariat à l'Energie Atomique, Note, CEA-N-2737 (ISSN 0429-3460). Fontenay-aux-Roses, France. http://inis.iaea.org/collection/NCLCollectionStore/_Public/25/063/25063370.pdf?r=1.

[47] Grenthe I., Plyasunov A.V., Spahiu K. (1997) Chapter IX. Estimations of medium effects on thermodynamic data (Grenthe I., Puigdomènech I., Eds.) Modelling in Aquatic Chemistry. OECD, Paris, France. p. 325. http://www.oecd-nea.org/dbtdb/pubs/book-pdf/325-426.pdf.

[48] Puigdomènech I., Plyasunov A.V., Rard J.A., Grenthe I. (1997) Chapter X. Temperature correction to thermodynamic data and enthalpy calculations (Grenthe I., Puigdomènech I.,

Eds.) Modelling in Aquatic Chemistry. OECD, Paris. p. 427. http://www.oecd-nea.org/dbtdb/pubs/book-pdf/427-494.pdf.
[49] Helgeson H.C. (1967) Thermodynamics of complex dissociation in aqueous solution at elevated temperatures. *J. Phys. Chem.* **71** 3121.
[50] Götz C., Geipel G., Bernhard G. (2008) Thermodynamical data of uranyl carbonate complexes from absorption spectroscopy (Merkel B.J., Hasche-Berger A., Eds.) Uranium, Mining and Hydrogeology. Springer, Berlin, Heidelberg, Germany. p. 907.
[51] Patterson C.S., Slocum G.H., Busey R.H., Mesmer R.E. (1982) Carbonate equilibria in hydrothermal systems: First ionization of carbonic acid in NaCl media to 300°C. *Geochim. Cosmochim. Acta* **46** 1653.
[52] Patterson C.S., Busey R.H., Mesmer R.E. (1984) Second ionization of carbonic acid in NaCl media to 250°C. *J. Solution Chem.* **13** 647.
[53] Oher H., Vercouter T., Réal F., Shang C., Reiller P.E., Vallet V. (2020) Influence of alkaline earth metal ions on structures and luminescent properties of $Na_mM_nUO_2(CO_3)_3^{(4-m-2n)-}$ (M = Mg, Ca; m, n = 0–2): time-resolved fluorescence spectroscopy and *ab initio* studies. *Inorg. Chem.* **59** 15036.
[54] Viard M., Gallay J., Vincent M., Meyer O., Robert B., Paternostre M. (1997) Laurdan solvatochromism: solvent dielectric relaxation and intramolecular excited-state reaction. *Biophys. J.* **73** 2221.
[55] Golub G.H., Van Loan C.F. (2013) Matrix computations. 4th, ed., The Johns Hopkins University Press, Baltimore.
[56] Ruckebusch C., Sliwa M., Pernot P., de Juan A., Tauler R. (2012) Comprehensive data analysis of femtosecond transient absorption spectra: A review. *J. Photochem. Photobiol. C: Photochem. Rev.* **13** 1.
[57] Ma J., Archirel P., Schmidhammer U., Teuler J.-M., Pernot P., Mostafavi M. (2013) Reduction of Earth Alkaline Metal Salts in THF Solution Studied by Picosecond Pulse Radiolysis. *J. Phys. Chem. A* **117** 14048.
[58] Ma J., Archirel P., Pernot P., Schmidhammer U., Le Caër S., Mostafavi M. (2016) Identification of Transient Radical Anions (LiClO4)n– (n = 1–3) in THF Solutions: Experimental and Theoretical Investigation on Electron Localization in Oligomers. *J. Phys. Chem. B* **120** 773.
[59] Bonin J., Lampre I., Pernot P., Mostafavi M. (2007) Solvation Dynamics of Electron Produced by Two-Photon Ionization of Liquid Polyols. II. Propanediols. *J. Phys. Chem. A* **111** 4902.
[60] Kerisit S., Liu C. (2010) Molecular simulation of the diffusion of uranyl carbonate species in aqueous solution. *Geochim. Cosmochim. Acta* **74** 4937.
[61] Kimuro S., Kirishima A., Kitatsuji Y., Miyakawa K., Akiyama D., Sato N. (2019) Thermodynamic study of the complexation of humic acid by calorimetry. *J. Chem. Thermodyn.* **132** 352.
[62] Li B., Zhou J., Priest C., Jiang D.E. (2017) Effect of salt on the uranyl binding with carbonate and calcium ions in aqueous solutions. *J. Phys. Chem. B* **121** 8171.
[63] Shannon R.D. (1976) Revised effective ionic radii and systematic studies of interatomic distances in halides and chalcogenides. *Acta Crystallogr., Sect. A* **32** 751.
[64] Marcus Y. (1985) Ion Solvation. Wiley, Chichester, UK.
[65] Claret F., Sakharov B.A., Drits V.A., Velde B., Meunier A., Griffault L., Lanson B. (2004) Clay minerals in the Meuse-Haute Marne underground laboratory (France): Possible influence of organic matter on clay mineral evolution. *Clays Clay Miner.* **52** 515.
[66] Dauzères A., Le Bescop P., Cau-Dit-Coumes C., Brunet F., Bourbon X., Timonen J., Voutilainen M., Chomat L., Sardini P. (2014) On the physico-chemical evolution of low-pH and CEM I cement pastes interacting with Callovo-Oxfordian pore water under its in situ CO2 partial pressure. *Cement Concrete Res.* **58** 76.

[67] Meinrath G. (1994) Aquatic Chemistry of Uranium. A Review Focusing on Aspects of Environmental Chemistry. Technische Universität Freiberg - Bergakademie. Freiberg, Germany. http://www.geo.tu-freiberg.de/fog/FOG_Vol_1.pdf.
[68] Atwood D.A. (2010) Radionuclides in the Environment. Wiley, Chichester, West Sussex, U.K. ; New York.
[69] Wang Y.H., Frutschi M., Suvorova E., Phrommavanh V., Descostes M., Osman A.A.A., Geipel G., Bernier-Latmani R. (2013) Mobile uranium(IV)-bearing colloids in a mining-impacted wetland. *Nat. Commun.* **4**. 2942.
[70]
[71] Janeczek J. (1999) Uranium : mineralogy, geochemistry and the environment (Burns P.C., Finch R., Eds.) Mineralogy and Geochemistry of Natural Fission Reactors in Gabon. De Gruyter, Washington, DC, USA. p. 321. http://www.minsocam.org/MSA/RIM/Rim38.html.
[72] Grivé M., Duro L., Colàs E., Giffaut E. (2015) Thermodynamic data selection applied to radionuclides and chemotoxic elements: An overview of the ThermoChimie-TDB. *Appl. Geochem.* **55** 85.
[73] Baker R.J. (2014) Uranium minerals and their relevance to long term storage of nuclear fuels. *Coord. Chem. Rev.* **266-267** 123.
[74] Thoenen T., Hummel W., Berner U., Curti E. (2014) The PSI/Nagra Chemical Thermodynamic Database 12/07. Paul Scherrer Institute, PSI Bericht Nr 14-04 (ISSN 1019-0643). Villigen, Switzerland. http://www.psi.ch/les/database.
[75] Maynard J.B. (1983) Geochemistry of Sedimentary Ore Deposits. *Geol. Mag.* **121** 370.
[76] Taylor G.H. (1980) Past oxygen levels: some evidence from uranium deposits (Trudinger P.A., Walter M.R., Ralph B.J., Eds.) Biogeochemistry of Ancient and Modern Environments. Springer, Berlin, Heidelberg. p. 65.
[77] Hostetler P.B., Garrels R.M. (1962) Transportation and precipitation of uranium and vanadium at low temperatures, with special reference to sandstone-type uranium deposits. *Econ. Geol.* **57** 137.
[78] Jensen M.L. (1958) Sulfur isotopes and the origin of sandstone-type uranium deposits. *Econ. Geol.* **53** 598.
[79] Rich R.A., Holland H.D., Petersen U. (1977) Hydrothermal Uranium Deposits. Elsevier, New York.
[80] Kimberley S.J., Kimberley M.M. (1978) Uranium Deposits, Their Mineralogy and Origin. University of Toronto Press, Mineral Association of Canada.
[81] Janeczek J., Ewing R.C., Thomas L.E. (1993) Oxidation of uraninite: Does tetragonal U3O7 occur in nature? *J. Nucl. Mater.* **207** 177.